

Quarterly Report for
July - September 1999
Stanford Geothermal Program
DE-FG07-95ID13370

Table of Contents

1. MEASUREMENTS OF STEAM-WATER RELATIVE PERMEABILITY	1
1.1 BACKGROUND	1
1.2 EXPERIMENTS	2
1.3 CONCLUSIONS	4
2. AN EXPERIMENTAL INVESTIGATION OF BOILING HEAT CONVECTION WITH RADIAL FLOW IN A FRACTURE	7
2.1 INTRODUCTION	7
2.2 THERMOCOUPLE ACCURACY VERIFICATION AND INSTALLATION	7
2.3 THERMAL CONDUCTIVITY OF HEAT FLUX SENSORS	8
2.4 FUTURE WORK	9
3. INFERRING ENDPOINT SATURATION FROM BOILING EXPERIMENTS AND FIELD MEASUREMENTS	11
3.1 INTRODUCTION	11
3.2 INFERRING ENDPOINT SATURATION FROM BOILING EXPERIMENTS	12
3.3 INFERRING ENDPOINT SATURATION FROM FIELD MEASUREMENTS	18
4. STEAM-WATER CAPILLARY PRESSURE	19
4.1 INTRODUCTION	19
4.2 THEORY	19
4.3 EXPERIMENTS	22
4.4 RESULTS	24
4.5 DISCUSSION	34
4.6 CONCLUSIONS	35
4.7 FUTURE WORK	35
5. ACCURATE MEASUREMENT OF STEAM FLOW PROPERTIES	37
5.1 SUMMARY	37

5.2 INTRODUCTION	37
5.3 EXPERIMENTS	37
5.4 RESULTS	41
5.5 CONCLUSIONS	45
5.6 FUTURE WORK	45
6. REFERENCES	47

1. MEASUREMENTS OF STEAM-WATER RELATIVE PERMEABILITY

This research project is being conducted by Research Associate Kewen Li, Huda Nassori, and Professor Roland Horne. The aim is to measure relative permeability relations for steam and water flowing simultaneously in rocks. We studied the effect of temperature on the measurement of fluid saturation in the core this quarter.

1.1 BACKGROUND

An X-ray CT technique has been used in recent years for measuring the distribution of steam and water saturation in rocks to obtain steam-water relative permeability curves (Satik and Horne, 1998, Mahiya, 1999). The steam saturation in a core sample during the measurement of steam-water relative permeability curves is usually calculated using the following equation:

$$S_{st} = \frac{CT_{wet} - CT_{exp}}{CT_{wet} - CT_{dry}} \quad (1.1)$$

where S_{st} is steam saturation; CT_{wet} , CT_{dry} are CT numbers of the rock when it is fully saturated by water and air, respectively; CT_{exp} is the CT number of the rock when it is partially saturated by steam.

It is known that CT number is density dependent, and density is temperature dependent, and CT number is therefore temperature dependent. Therefore, temperature may significantly affect the calculation of steam saturation in rocks. Little attention, however, has been paid to the effect of temperature on the CT number and then the calculation of steam saturation in a core sample.

The values of CT_{exp} are usually measured at high temperatures during the measurement of steam-water relative permeability curves. If the values of CT_{wet} were measured at room temperature, CT_{exp} would be less than CT_{wet} even when there is no steam at all in the rock. Therefore, the steam saturation calculated using Equation 1.1 would be greater than zero. The experimental results in this report showed that the error of steam saturation could be over 10 percent if the effect of temperature on CT number were not considered. Based on this fact, the method for calculating steam saturation was modified to be:

$$S_{st} = \frac{CT_{wet}(T) - CT_{exp}(T)}{CT_{wet}(T) - CT_{dry}(T)} \quad (1.2)$$

where T is the temperature in rock-fluid systems.

The main idea in Equation 1.2 is that all the values of CT number for calculating steam saturation, CT_{wet} , CT_{exp} , and CT_{dry} , should be measured at the same temperature. The effect of temperature on CT_{wet} and CT_{exp} can not be compensated by the effect of temperature on CT_{wet} and CT_{dry} for calculating steam saturation using Equation 1.2.

Once the values of $CT_{wet}(T)$ and $CT_{dry}(T)$ are obtained, porosity can be then calculated using the following equation:

$$\phi = \frac{CT_{wet}(T) - CT_{dry}(T)}{CT_{water}(T) - CT_{air}(T)} \quad (1.3)$$

where CT_{water} and CT_{air} are the CT numbers of water and air at a temperature of T , respectively.

Since porosity does not change much with temperature, we could use the values of CT numbers at a room temperature to calculate the porosity of a core sample.

We measured the values of CT_{wet} and CT_{dry} along the core at different temperatures in order to study the effect of temperature on fluid saturation measured using X-ray CT technique. The experimental results confirmed that all the values of CT number should be measured at the same temperature otherwise significant error will occur in the calculation of steam saturation.

1.2 EXPERIMENTS

Distilled water was used in this study; the specific gravity and viscosity were 1.0 and 1.0 cp at 20°C. The core used was a fired Berea at a high temperature; its permeability and porosity were 1460 md and 24.7%; the length and diameter were 43.2 cm and 5.04 cm, respectively. This core and its coreholder were the same as used by Mahiya (1999). The apparatus used for investigating the effect of temperature on the calculation of fluid saturation is also similar to that used by Mahiya (1999). The only difference is that constant temperature was kept by using Lab View systems through the flexible guard heater instead of zero heat loss.

The core preparation procedure involved drying the core by subjecting it to 120°C using the flexible guard heater and simultaneously evacuating. Once dried, a dry X-ray scan was then made to obtain the CT attenuation values CT_{dry} at a specific high temperature. After the temperature was decreased to a certain value, another dry X-ray scan was made to obtain the CT attenuation values CT_{dry} at a different temperature. This procedure was repeated until the values of CT_{dry} at room temperature were obtained. The core was then fully saturated with water and scanned to obtain the values of CT_{wet} at room temperature, and from these the porosity distribution was obtained. The next step was to increase the temperature to a certain value and another wet X-ray scan was made to obtain the CT attenuation values CT_{wet} at this temperature. This procedure was repeated at different temperatures.

The porosity distribution along the core is shown in Figure 1.1. We measured the porosity distribution two times because of the position shift of the coreholder system brought about by the maintenance of the CT machine. The position for the second measurements was tried to put in the same one as the first time. Figure 1.1 shows that the two porosity measurements were consistent with each other except at the bottom end of the core. The values of the average porosity measured in two times were 24.7 and 24.8 %, respectively.

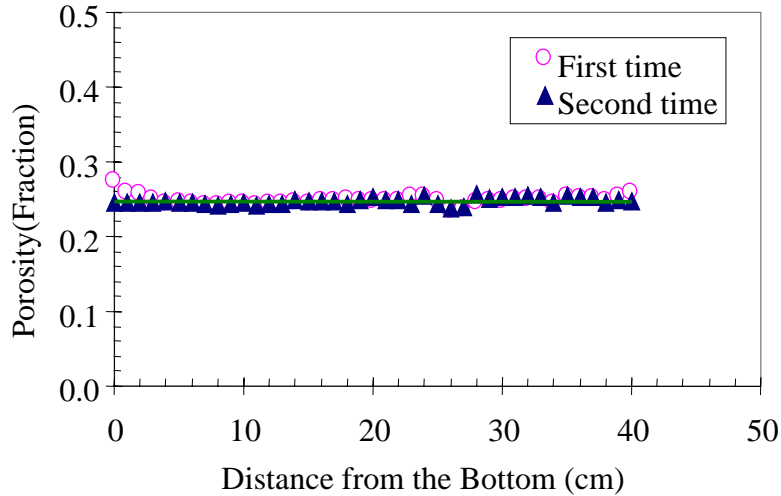


Figure 1.1: Porosity distribution along the core.

The effect of temperature on the values of CT_{dry} is shown in Figure 1.2. It is clear that there is a significant difference among the values of CT_{dry} at different temperatures.

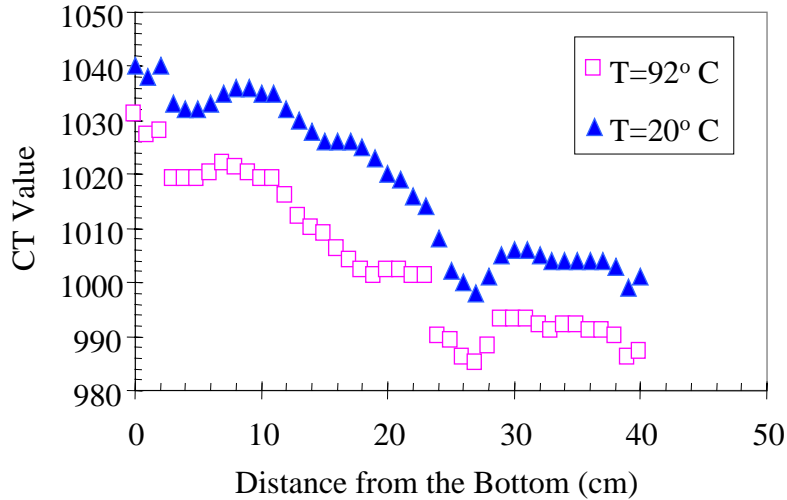


Figure 1.2: Effect of temperature on the values of CT_{dry} .

Figure 1.3 shows the effect of temperature on the values of CT_{wet} when the core was fully saturated with water at four different temperatures. The values of CT_{wet} increase with the decrease of temperature. The temperature of the rock-fluid systems during the measurement of steam-water relative permeability curves is usually around or higher than 120°C . Therefore the effect of temperature on the values of CT_{wet} at that temperature will be more significant than that shown in Figure 1.3.

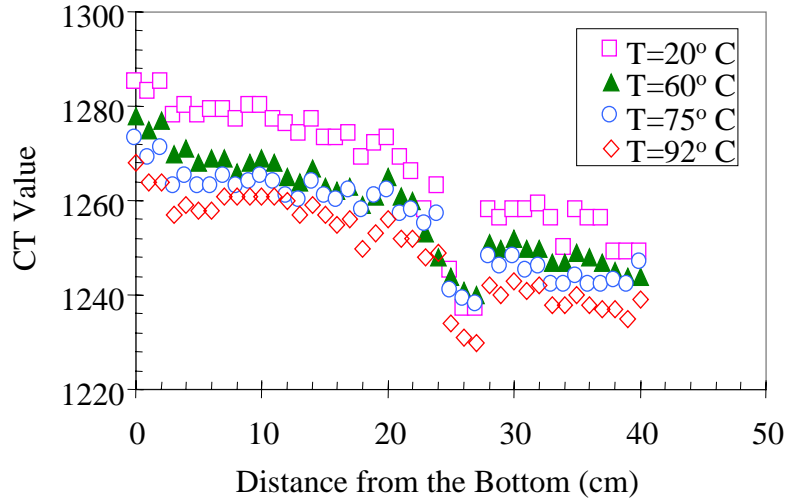


Figure 1.3: Effect of temperature on the values of CT_{wet} .

If the values of CT_{wet} and CT_{dry} were measured at room temperature and the values of CT_{exp} were measured at the experimental temperature (say 92°C), and if the steam saturation was then calculated using Equation 1.1 then the results would be as in Figure 1.4.

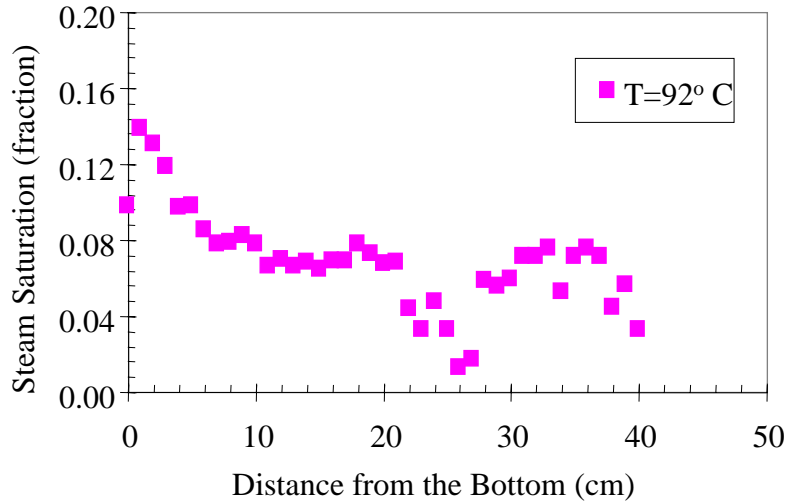


Figure 1.4: Effect of temperature on the calculation of steam saturation.

Figure 1.4 shows that the error for calculating steam saturation at a temperature of 92°C (no steam exists at this temperature in a rock fully saturated with water) can be more than 10 percent if the temperature effect were not considered. The error was about 5 percent at a temperature of 65°C .

1.3 CONCLUSIONS

1. There is a significant effect of temperature on the values of CT numbers of a core-fluid system that are used to calculate steam or water saturation.
2. The values of CT numbers of a core-fluid system that are used to calculate steam or water saturation should be measured at the same temperature.

The absolute error of calculating steam saturation may be over 10 percent if the temperature effect is not considered.

2. AN EXPERIMENTAL INVESTIGATION OF BOILING HEAT CONVECTION WITH RADIAL FLOW IN A FRACTURE

This project is being conducted by Research Assistant Robb Barnitt and Professor Roland Horne. The goal is to investigate and compare the heat flux and temperature gradients that develop during boiling with liquid injection into a rock fracture in a geothermal reservoir. Ultimately, this project intends to develop a boiling convection coefficient for use in calculating heat transfer with boiling in fractured geothermal rock. Improved understanding and modeling of heat transfer in a fracture will ultimately lead to better strategies for injection into geothermal reservoirs.

2.1 INTRODUCTION

Work conducted this quarter focussed on preparing the experimental apparatus for the upcoming rerun of the aluminum disk experiment, and subsequent graywacke disk experiment. Some modifications and improvements were made to the apparatus itself, and the experimental equipment used in data collection were checked or replaced in an attempt to rectify previous problems. In previous experiments, the heat flux sensors failed at approximately $10,000 \text{ W/m}^2$. In addition, problems associated with electrical grounding of the experimental equipment were experienced. The data acquisition system was consequently replaced, rewired and grounded. New heat flux sensors were selected and thermocouple accuracy verified.

2.2 THERMOCOUPLE ACCURACY VERIFICATION AND INSTALLATION

For the upcoming experiments, the experimental apparatus design remains largely unchanged. Eight 1.0 mm diameter T-type thermocouples will be installed in the aluminum disk at varying distances from the fracture surface, and will record the temperature gradients that develop as water flashes to steam in the fracture. Calculation of the boiling convection coefficient requires that the surface temperature (T_{surf}), on the top of the aluminum disk and in the fracture, be known. This was calculated previously by linear interpolation of the linear temperature gradient which developed axially in the aluminum disk. To achieve the value of T_{surf} in future experiments, thin 12.5 micron thick cementable thermocouples were purchased and installed. Three such thermocouples were attached to the fracture surface using a cement of high thermal conductivity, spaced 120 degrees apart, and oriented 1.5 cm from the disk center.

To verify the accuracy of the larger diameter thermocouples to be reused in the upcoming experiments, a controlled experiment to verify their accuracy was performed. The thermocouples were bundled with a J-type thermocouple that served as a control. Following insertion in a laboratory oven, a series of temperatures were achieved, and temperature data recorded. Each thermocouple's deviation from the control was plotted at each of the experimental temperatures. Deviation increased linearly with increasing temperature. This data will be utilized for data adjustment.

2.3 THERMAL CONDUCTIVITY OF HEAT FLUX SENSORS

To calculate the experimental heat flux accurately, the thermal conductivity (k) of each heat flux sensor must be ascertained as input into the data acquisition software. Several replacement heat flux sensors were examined to determine their suitability for the upcoming experiment and determine their thermal conductivity.

In a chilled water bath at a constant temperature 9.8 degrees C, a beaker containing two heat flux sensors, a heater, and insulation was submerged. The orientation of each item is illustrated in Figure 2.1.

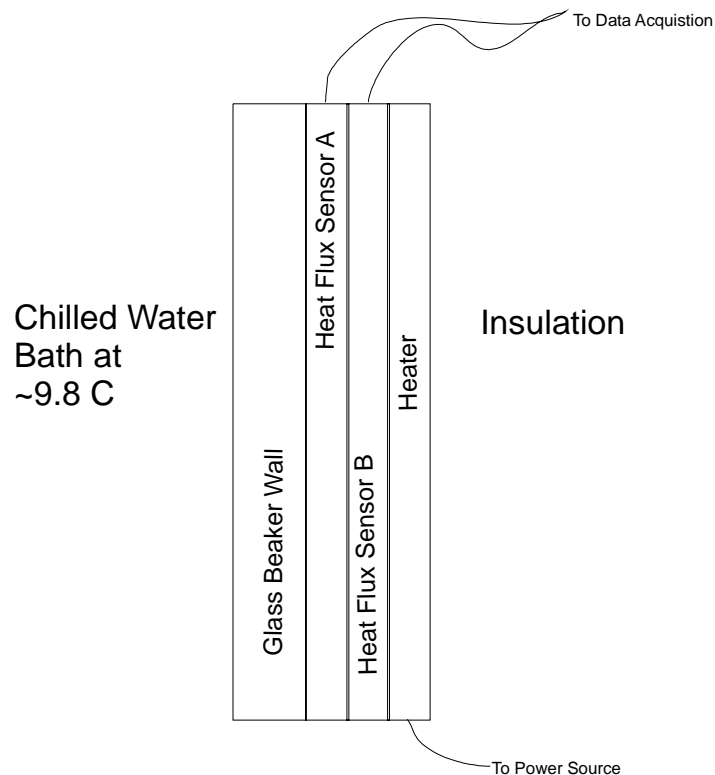


Figure 2.1: Heat flux sensor k calculation experiment.

Heat flux sensors A and B were stacked on top of one another, and backed by a heat source. Insulation packed behind the heater simulated one-dimensional heat flow toward the cold water bath. Heat flux data were collected from the known (A) and experimental (B) heat flux sensors over a range of voltages and currents. The data acquisition software was used to match the W/m^2 output of each heat flux sensor by varying the k of heat flux sensor B. Using this procedure, two replacement heat flux sensors were selected for use in the upcoming experiments.

2.4 FUTURE WORK

The experiment executed previously using the aluminum disk will be repeated. This will provide additional data points to observe the behavior of heat flux and boiling convection coefficient variance with injection rate. If the 12.5 micron diameter thermocouples cemented to the surface upon which boiling occurs prove to be successful, these thermocouples will also be employed in the future graywacke disk experiment.

Another length of Geysers core has been received for use in rerunning the experiment with a graywacke disk prepared similarly to the sandstone and aluminum disks. The new graywacke disk will be prepared using a surface grinder, and drilled to specification.

Previous experimental results indicated that low porosity and low permeability Geysers graywacke behaves unlike the sandstone or aluminum. The temperature gradient indicated that vaporization occurred beneath the fracture surface, isolating the boiling in the pores from the flow conditions in the fracture. Although this general behavior is expected again, the temperature gradients will be measured to a refined degree of accuracy compared to the original experiment. Additionally, a clearer relationship between observed behavior and collected data will be available for comparison between all three experimental materials.

3. INFERRING ENDPOINT SATURATION FROM BOILING EXPERIMENTS AND FIELD MEASUREMENTS

This project is being conducted by Research Assistant, Rodolfo Belen Jr. and Prof. Roland Horne. The aim is to determine the endpoint saturation of steam and liquid water relative permeability curves of geothermal reservoir rocks.

3.1 INTRODUCTION

Relative permeability is important in describing the flow of two-phase steam in geothermal reservoirs. Presently, however, relative permeability relations for steam and liquid water are not completely understood. Permeability relations are normally adopted from field data or from nitrogen and water flow experiments.

The experimental determination of steam and liquid water relative permeabilities is a central target of the Stanford Geothermal Program. Flow-through experiments on Berea sandstones were performed by Ambusso (1996), Satik (1998) and Mahiya (1999) using X-ray computer tomography to determine steam saturation profiles. In a different approach, numerical simulation was used by Guerrero et al. (1998) to infer relative permeabilities of Berea sandstones, based on temperature, pressure, and steam saturation data obtained from steady state boiling experiments performed by Satik (1997).

All of these earlier studies used Berea sandstone in order to capitalize on its larger permeability relative to geothermal rocks, which enabled the experiments to be performed in reasonable time. This study aims to extend the understanding to low permeability geothermal rocks by determining only the endpoint saturations of the relative permeability curves. The endpoint or irreducible or immobile saturation of a certain phase is the saturation at which that phase becomes mobile in multiphase flow.

Combining information about the endpoint saturations from the “slow” geothermal rock experiments with information about the general shape of the relative permeability curves from the “faster” sandstone rock experiments will completely define the steam-liquid water relative permeability behavior.

Furthermore, determination of the irreducible water saturation will provide a better understanding of the fluid storage capacities of geothermal rocks. This will be valuable in estimating the size of the available resource in vapor-dominated reservoirs as well as liquid-dominated reservoirs that are experiencing dry out as a result of exploitation.

The objective of this study is to determine the endpoint saturation of the steam and liquid water relative permeability curves in geothermal rocks by inference from pressure, temperature and saturation data obtained from boiling experiments as well as by inference from field measurements of temperature and flowing enthalpy. Furthermore, this study also aims to design and perform flash experiments using Berea sandstone cores that will allow the experimental determination of the endpoint water saturation and the confirmation of the field techniques.

3.2 INFERRING ENDPOINT SATURATION FROM BOILING EXPERIMENTS

Results of previous steady-state boiling experiments performed by Satik (1997) were analyzed to investigate whether endpoint saturations can be inferred from the experimental data obtained.

3.2.1 Experimental Design of Boiling Experiments

In 1996 and 1997, Satik performed a series of experiments using Berea sandstone cores. The objective of the study was to further the understanding of the boiling process in porous media and ultimately to obtain capillary pressure functions and relative permeability relations for steam and liquid water. The steady-state boiling experiments involved the heating of a rock saturated with liquid water and observation of the boiling process by continuous measurement of pressure, temperature, heat flux and steam saturation within the rock. The X-ray CT scanner was used to visualize the boiling process and to determine the three-dimensional fluid distributions within the rock. The experimental arrangement (Figure 3.1) and procedure were described in detail in the last quarterly report.

The boiling experiments are analogous to drainage experiments in oil and water systems, in which oil, the non-wetting fluid, is injected into a rock saturated with water, the wetting fluid, to displace the water from the rock. However, in this case, steam produced by heating the water-saturated rock displaces the liquid water from the rock.

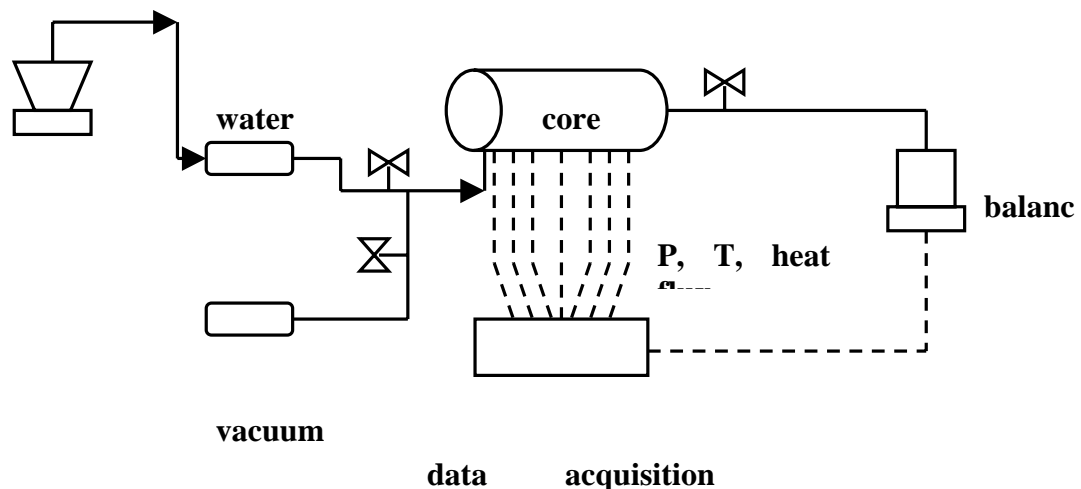


Figure 3.1: Configuration of boiling experiments.

3.2.2 Results of Boiling Experiments

As the heating rate was increased, the steady state steam saturation profile indicated a progressive boiling process with the formation of distinct regions of steam, two-phase and liquid water. Figure 3.2 is the steam saturation profile of one of the vertical experiments performed by Satik (1997) showing the formation of steam, two-phase and liquid regions within the core as the heating rate is increased. The sudden drop in the steam saturation near the heater end of the core that marks the transition from steam to two-phase conditions is designated here as the elbow in the saturation profile.

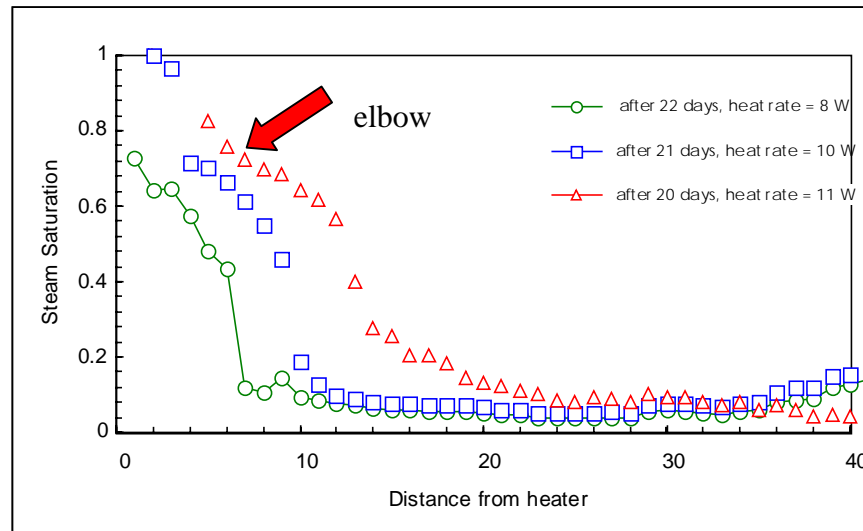


Figure 3.2: Steam saturation profile vertical boiling experiment, Satik, Spring 1997.

3.2.3 Sensitivity Analysis of Boiling Experiments

It is hypothesized that the irreducible water saturation can be correlated with the observed elbow in the steam saturation profile. Analyzing the sensitivity of the boiling process to the irreducible water saturation through numerical modeling will test the validity of this hypothesis. The boiling process was simulated using different values of the endpoint water saturation of the relative permeability curves. The pressure, temperature and saturation profiles were predicted to verify if the elbow in the saturation profiles could be correlated with the irreducible water saturation.

In 1998, Guerrero et al. developed a two-dimensional radial iTOUGH2 model to infer relative permeability relations from the results of the boiling experiments. The same model was used in the sensitivity analysis but the grids were refined to give a better resolution of the variations in the steam saturation near the heater end of the core.

Forward calculations in iTOUGH2 were performed to predict the pressure, temperature, and steam saturation profiles along the core. It is assumed that linear steam-liquid water

relative permeability functions and Leverett capillary functions govern the flow of two-phase steam in the sandstone core.

The non-adiabatic boiling process was simulated using varying heating rates as illustrated in Figure 3.3 and using three different values of endpoint water saturation: 0.1, 0.2, and 0.5. Steam saturation was then plotted at 0.2-cm. intervals and up to a distance 5 cm. away from the heater end. The profiles at various times are shown in Figures 3.4 to 3.6.

It is evident from the plots that the steam and two-phase regions expand as the heating rate is increased and as time progresses. As the heating rate is increased, boiling commences and steam and two-phase regions form.

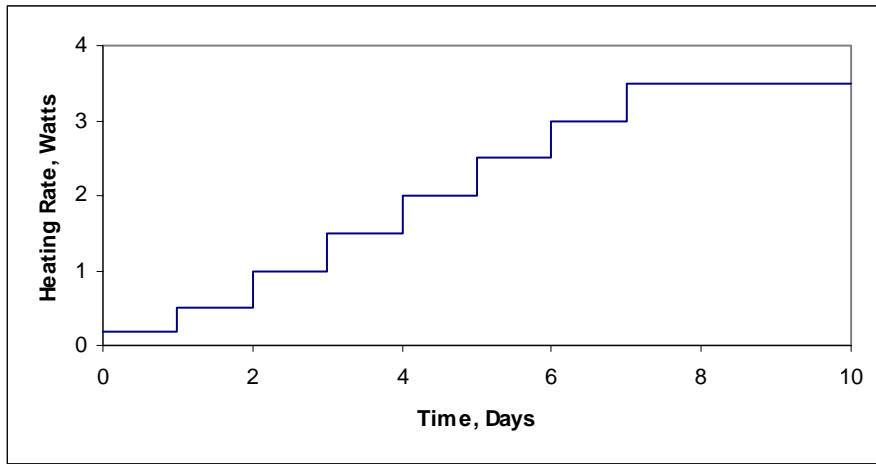


Figure 3.3: Heating rate as a function of time.

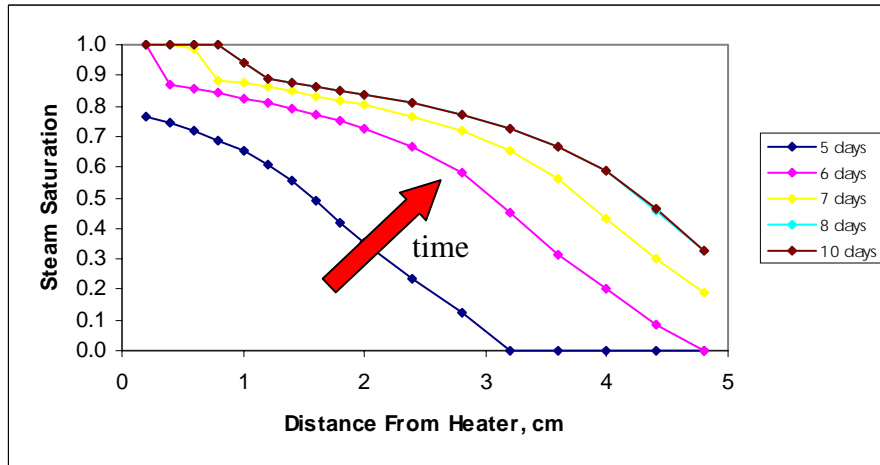


Figure 3.4: Steam saturation profile: endpoint water saturation = 0.1.

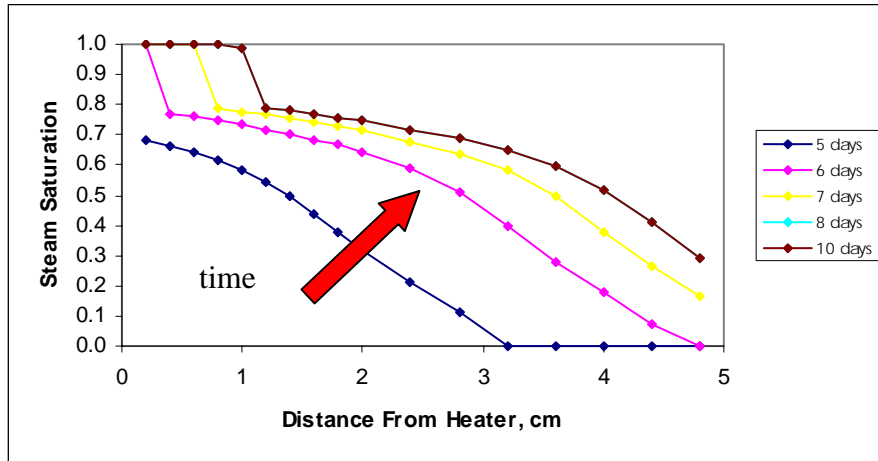


Figure 3.5: Steam saturation profile: endpoint water saturation = 0.2.

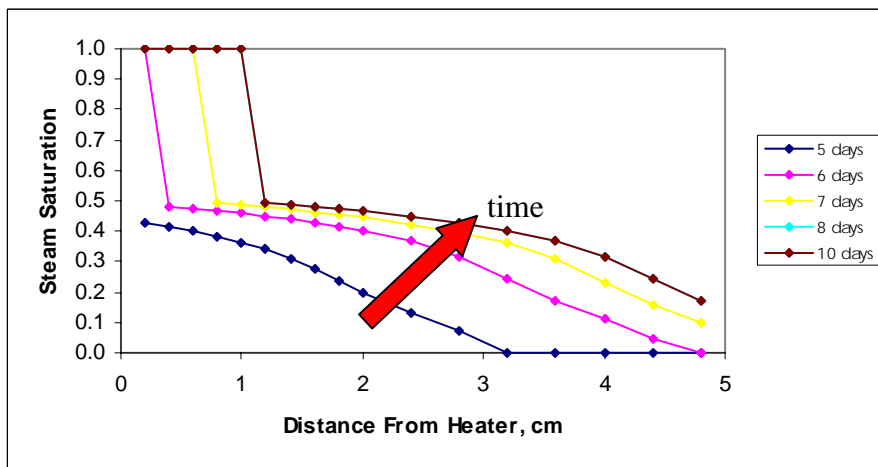


Figure 3.6: Steam saturation profile: endpoint water saturation = 0.5.

The simulation results indicate a correlation between the elbow in the steam saturation profile and the endpoint water saturation. In all three cases, the steam region extends to a distance 1 cm. from the heater end. An abrupt drop in the steam saturation to a value close to the assumed endpoint water saturation marks the transition to two-phase conditions. This drop in steam saturation corresponds to the elbow in the profile. The steam saturation stays close to this value behind the elbow and then further goes down with distance away from the heater end.

It is important to note a few points about the modeling procedure and results. First, it was not possible to raise the heating rate to greater than 4 W because further increasing the heating rate resulted in convergence failures in the modeling runs. Second, steady state conditions were reached after about ten days of heating the core. Steady state means that the simulated steam saturation, pressure and temperature profiles remain invariant with time. As a consequence, the simulated steam saturation profiles indicate steam conditions in the region starting from the heater end to a distance 1 cm. away. Beyond

this region, the simulated steam saturation profiles indicate two-phase and liquid conditions.

3.2.4 Inferred Endpoint Water Saturations

Figures 3.2, 3.7 to 3.9 show the steam saturation profiles obtained from the boiling experiments that were conducted by Satik in Spring and Summer 1997. The figures show the steam saturation profile with distance along the core and as a function of the heating rate. It is important to note that steam saturation, pressure and temperature were measured only at 1-cm intervals along the core.

It can be inferred from the experimental results that the irreducible water saturation of Berea sandstone is about 0.8. This inference is based on the observed elbow in the steam saturation profiles.

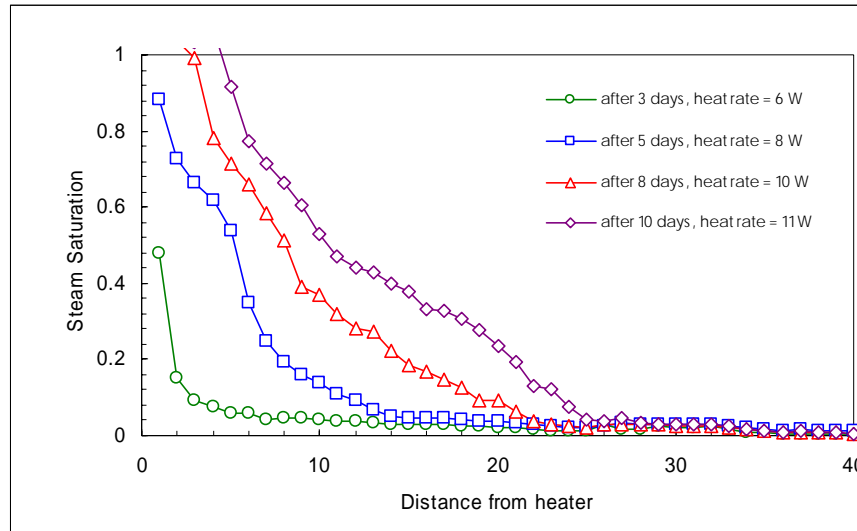


Figure 3.7: Steam saturation profile horizontal boiling experiment, Satik, Summer 1997.

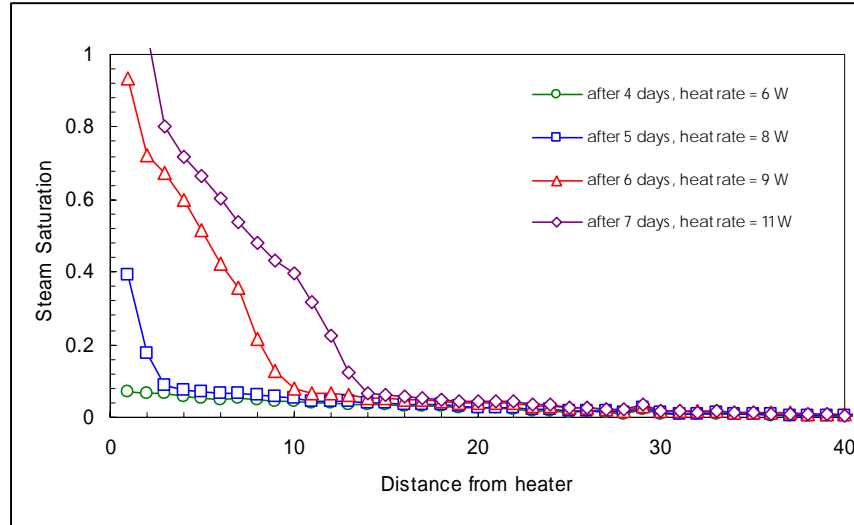


Figure 3.8: Steam saturation profile: top-heating vertical boiling experiment, Satik, Summer 1997.

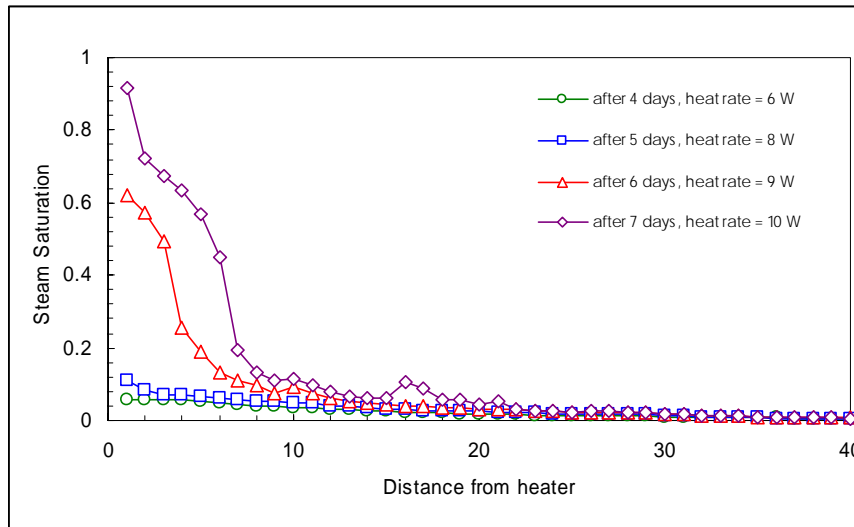


Figure 3.9: Steam saturation profile: bottom-heating vertical boiling experiment, Satik, Summer 1997.

3.2.5 Future Work

Future work will be directed toward designing boiling experiments using lower permeability geothermal reservoir rocks, which will involve numerical modeling of the boiling process for the case of tighter geothermal reservoir rocks. Furthermore, it is intended to solve the problem causing the convergence errors when higher heating rates are imposed in the numerical model. It is also intended to study the sensitivity of the boiling process to the irreducible steam saturation.

3.3 INFERRING ENDPOINT SATURATION FROM FIELD MEASUREMENTS

Steam production during the exploitation of vapor-dominated geothermal reservoirs greatly exceeds what the reservoir can store as vapor. Therefore, these reservoirs must contain substantial amounts of liquid water to sustain production (James, 1968; Nathenson 1975; Grant, 1979). In describing the response of vapor-dominated reservoirs to exploitation, it is valid to assume that the liquid water is completely immobile. Although water may be slightly mobile in the natural state of the reservoir, it is soon immobile because the water saturation drops as fluids are produced (Grant, 1979). The liquid water is adsorbed in the pores of the reservoir matrix and is able to vaporize, but is not able to flow as liquid water.

Grant (1979) estimated the in-place water saturation of the Kawah Kamojang geothermal reservoir based on variations in the gas content of the production fluids. Changing the flow rate at the wellhead produces a response in the reservoir pressure and gas content, which allows for the estimation of the in-place water saturation or the endpoint water saturation of the reservoir rock. In contrast, this study aims to infer the endpoint saturations from field measurements of changes in the flowing enthalpies and production rates of producing wells.

Flow and lumped-parameter models can be used to describe the pressure, temperature and saturation distributions accompanying production. In the Spring Quarter report, the flow model used by Grant to infer the in-place water saturation of the Kawah Kamojang geothermal reservoir was presented. This study aims to develop a model that will be used to infer the endpoint water saturation using field production data.

Future work will be directed toward developing a model that will be used to infer endpoint water saturation using field production data. This will involve modeling of two-phase radial flow to obtain pressure and saturation profiles with time and radial distance. The modeling results will provide a deeper insight on the estimation of the reservoir saturation using field measurements. Furthermore, it is intended to extend the model to liquid-dominated reservoirs that produce two-phase steam. The goal is to extrapolate the endpoint water saturation of the reservoir rocks using field production data.

4. STEAM-WATER CAPILLARY PRESSURE

This research project is being conducted by Research Associate Kewen Li and Professor Roland Horne. The final objective is to find a method for measuring steam-water capillary pressure in rocks. As a preliminary step, we are studying the imbibition behavior of water into air-saturated rocks in order to verify the method developed for calculating steam-water capillary pressure.

4.1 INTRODUCTION

Last quarter (April-June 1999), we measured the imbibition properties of water into air-saturated porous media from a very low permeable chalk (about 5 md) to a very highly permeable glass-bead pack (about 25 darcy). It was found from these experimental results that the relationship between the imbibition rate and the reciprocal of recovery by water imbibition was linear in both the low permeable chalk and the highly permeable unconsolidated porous media. All those experiments, however, were conducted in porous media with zero initial water saturation. In this quarter, we measured the imbibition properties of water into a sandstone sample at different values of initial water saturation. An X-ray CT technique was used to measure the distribution of water saturation inside the core sample and to monitor the establishment of initial water saturation. We found that the maximum water saturation after the water imbibition in the core was varied very little with initial water saturation. It may be the capillary pressure at the water saturation behind the water imbibition front that controlled the process of water imbibition into the core sample. Therefore, the capillary pressures calculated from the water imbibition data were the same at different initial water saturations.

4.2 THEORY

The method for calculating gas-water capillary pressure from measurements of water imbibition at zero initial water saturation was described in the quarterly report for January-March 1999. In the current quarter, we developed the method for calculating gas-water capillary pressure at some initial water saturation.

Assuming Darcy's law during the process of the spontaneous water imbibition that occurs vertically upward in a core with a certain initial water saturation, the water imbibition velocity is expressed as:

$$v_w = -\frac{k_w}{\mu_w} \left(\frac{\partial p_w}{\partial x} + \rho_w g \right), \quad (4.1)$$

where v_w and k_w are the flowing velocity and the effective permeability of water phase, respectively; ρ_w and μ_w are water density and viscosity; p_w is the pressure of water phase at the position x . From the definition of capillary pressure, the pressure of water phase can be calculated:

$$p_w = p_g - p_c, \quad (4.2)$$

Substituting Eq. 4.2 into Eq. 4.1:

$$v_w = \frac{k_w}{\mu_w} \left(\frac{\partial p_c}{\partial x} - \frac{\partial p_g}{\partial x} - \rho_w g \right), \quad (4.3)$$

where p_g is the pressure of gas phase and p_c is capillary pressure.

During the water imbibition, gas mobility is usually much greater than water mobility. If gas mobility is assumed to be infinite, gas pressure gradient is estimated as:

$$\frac{\partial p_g}{\partial x} = -\rho_g g, \quad (4.4)$$

where ρ_g is gas density. Substituting Eq. 4.4 into Eq. 4.3:

$$v_w = \frac{k_w}{\mu_w} \left(\frac{\partial p_c}{\partial x} - \Delta\rho g \right), \quad (4.5)$$

where $\Delta\rho$ is the density difference between gas and water.

Schembre, et al. (1998) used the X-ray CT method to monitor the process of water imbibition into air-saturated rocks that were assembled vertically upward; and reported that the CT images of diatomites and chalk showed a homogeneous and piston-like water front during the water imbibition. Our experimental results also showed that water imbibition would be a piston-like flow process. Based on these experimental observations, we can conclude that water does imbibe into air-saturated rocks in a piston-like manner in certain cases. In a piston-like flow, the following equation holds:

$$\frac{\partial p_c}{\partial x} = \frac{p_c}{x}, \quad (4.6)$$

Substituting Equation. 4.6 into Equation 4.5:

$$v_w = \frac{k_w}{\mu_w} \left(\frac{p_c}{x} - \Delta\rho g \right), \quad (4.7)$$

The accumulated volume of water imbibed into the core with initial water saturation can be calculated using the following equation:

$$N_{wt} = Ax\phi(S_w - S_{wi}), \quad (4.8)$$

where A and N_{wt} are the cross-section area of the core and the volume of water imbibed into the core, respectively; ϕ is porosity; S_w and S_{wi} are the water saturation behind the water front and the initial water saturation in the core. The water imbibition rate Q_w is equal to Av_w . Therefore, Equation 4.7 can be expressed as:

$$Q_w = \frac{Ak_w}{\mu_w} \left(\frac{p_c}{x} - \Delta\rho g \right), \quad (4.9)$$

Substituting Equation. 4.8 into Equation 4.9:

$$Q_w = \frac{A^2 \phi k_w (S_w - S_{wi}) p_c}{\mu_w} \frac{1}{N_{wt}} - \frac{Ak_w}{\mu_w} \Delta\rho g, \quad (4.10)$$

Arrange Equation 4.10:

$$Q_w = \frac{dN_{wt}}{dt} = a \frac{1}{\eta} - b, \quad (4.11)$$

where:

$$a = \frac{Ak_w (S_w - S_{wi})}{\mu_w L} p_c, \quad (4.12)$$

$$b = \frac{Ak_w}{\mu_w} \Delta\rho g, \quad (4.13)$$

and

$$\eta = \frac{N_{wt}}{V_p}, \quad (4.14)$$

where V_p and L are the length and the pore volume of the core sample, respectively; η the imbibition recovery of gas.

Based on Equations 4.12 and 4.13, capillary pressure can be calculated:

$$p_c = \frac{1}{(S_w - S_{wi})} \frac{a}{b} \Delta\rho g L, \quad (4.15)$$

The values of a and b in Equation 4.15 can be calculated from the plot of imbibition rate and the reciprocal of imbibition recovery. S_w can be measured during the water imbibition test. Hence, we can compute capillary pressure using Equation 4.15.

According to Equation 4.13, the effective water permeability at the water saturation of S_w can be computed using the following equation:

$$k_w = \frac{\mu_w}{A\Delta\rho g} b, \quad (4.16)$$

A great challenge in characterizing imbibition behavior in gas-liquid systems was to calculate capillary pressure p_c and effective water permeability k_w separately. Handy (1960) and Schembre, et al. (1998) characterized spontaneous imbibition using the following equation:

$$N_{wt}^2 = A^2 \frac{p_c k_w \phi S_w}{\mu_w} t, \quad (4.17)$$

There were three disadvantages to the use of Equation 4.17 for characterizing spontaneous imbibition. First, capillary pressure and effective water permeability could not be calculated separately from the spontaneous water imbibition test. Secondly, the straight line between the square of weight gain N_{wt} and time t often did not go through the origin point, as prescribed by Equation 4.17. Thirdly, the relationship between the square of weight gain N_{wt} and time t was not a straight line in some cases, especially for highly permeable samples. Application of Equations 4.15 and 4.16 for characterizing spontaneous imbibition may be a solution to these problems.

The rate of water imbibition into rocks is primarily dependent on the wettability of the rock, permeability, pore structure, and the interfacial tension between the imbibed phase and the resident phase. The study of spontaneous water imbibition is fundamental to water injection performance in low permeability reservoirs such as geothermal reservoirs. Therefore, the method developed in this study is of importance in characterizing spontaneous water imbibition and scaling the experimental data even though it may not be used to calculate the whole capillary pressure curve.

4.3 EXPERIMENTS

Distilled water was used as the liquid phase in this study since the clay in the core was removed by firing. The permeability and porosity of the sandstone sample was around 1200 md and 24.5%; its length and diameter were 43.5 cm and 5.06 cm. The data acquisition software used in the equipment for measuring water imbibition into the core with different initial water saturation was LabView 4.1 by National Instrument Company. A schematic of the apparatus is shown in Figure 4.1.

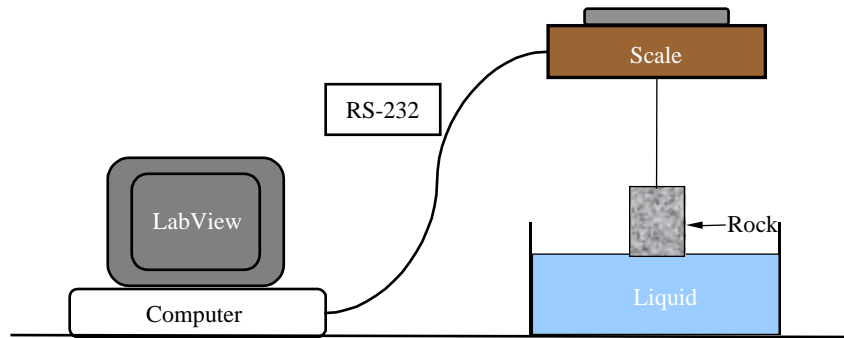


Figure 4.1: Schematic of apparatus for imbibition test.

Since the core used in this study was long and its weight was beyond the range of Mettler balance used last quarter, another balance (Sartorius, Model BP6100) with a larger capacity was used for the imbibition tests. This balance has an accuracy of 0.1g and a range from 0 to 6100 g. The core sample was hung under the balance. The amount of water imbibed into the core was measured over time using an under-weighing method and the real-time data was recorded continuously by a computer through the RS-232 interface. The purpose of the under-weighing method is to reduce the experimental error caused by water evaporation from the water container. However, there may be still water evaporation from the surface of the rock. Therefore, we conducted two different types of water imbibition tests (with and without heat-shrink tubing wrapped around the core) at zero initial water saturation.

The X-ray CT scanner used in this study for measuring the distribution of water saturation along the core was a PickerTM 1200 SX X-ray CT scanner with 1200 fixed detectors. The voxel dimension is 0.5 mm by 0.5 mm by 5 mm, the tube current used in this study was 50 mA, and the energy level of the radiation was 140 keV. The acquisition time of one image is about 3 seconds while the processing time is around 40 seconds.

The apparatus for measuring gas-water relative permeability curves developed by Li and Horne (1999) was used for establishing certain initial water saturation; its schematic is shown in Figure 4.2.

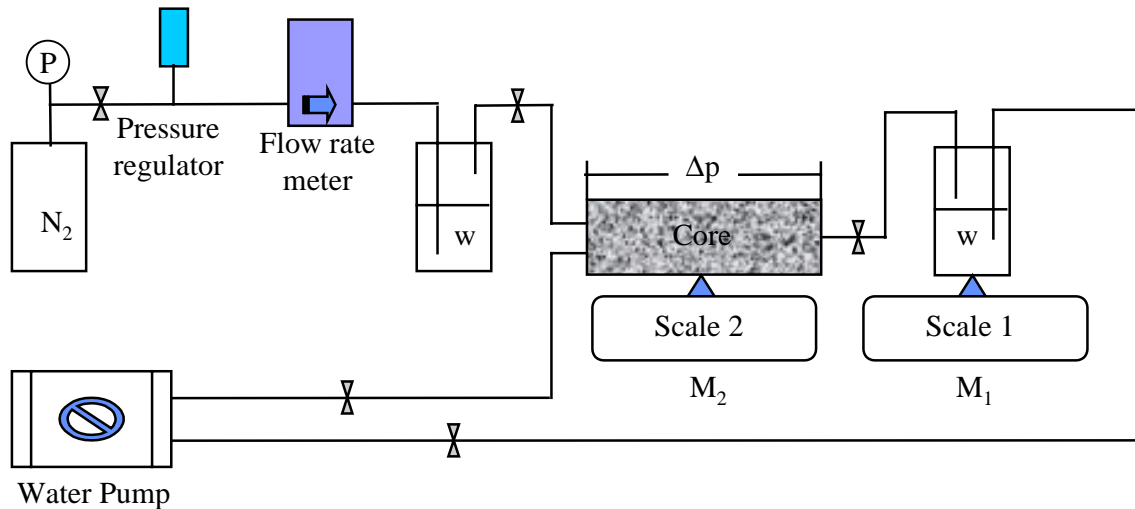


Figure 4.2: Schematic of gas-water relative permeability steady-state test.

The core sample was dried by heating to a temperature of 105°C in an oven until its weight did not vary during eight hours. The core was then assembled in the apparatus after it was cooled down, as shown in Figure 4.1. Water started to imbibe into the core once the bottom of the core was brought in contact with the water surface by raising the water container. The weight change of the core sample was then recorded in time and used to calculate capillary pressure.

After the water imbibition test at zero initial water saturation for the core without heat-shrink tubing wrapped around, the core was dried again and wrapped with heat-shrink tubing. Two end plates with holes through were installed at the inlet and outlet of the core for fluid injection. The heat-shrink tubing and the two end plates worked as a coreholder. The measurement of water imbibition test was repeated at zero initial water saturation to compare with the case without heat-shrink tubing wrapped around the core. Following that, the core was installed in the apparatus shown in Figure 4.2 for the establishment of an initial water saturation. The average water saturation in the core was monitored by the balance under the core system; the distribution of water saturation was then measured using the CT scanner. When the magnitude and the distribution of the water saturation in the core were satisfactory, the core was assembled in the apparatus shown in Figure 4.1 to do the water imbibition test at this initial water saturation.

4.4 RESULTS

Figure 4.3 shows the results of water imbibition into the air-saturated core with and without heat-shrink tubing wrapped around. It can be seen from Figure 4.3 that the water gain in the core with closed boundary condition (with heat-shrink tubing) was greater than that with open boundary condition. This may be due to the evaporation of water on the side surface of the rock since the area of rock surface was very large, about 683 cm². To avoid this problem, all other water imbibition tests at different initial water saturations were run with the closed boundary conditions.

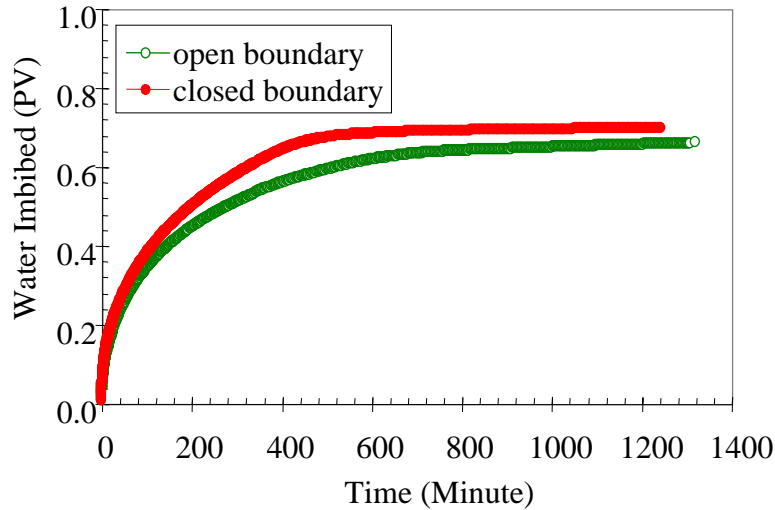


Figure 4.3: Water imbibition vs. time in the core at different boundary conditions.

The relationship between the water imbibition rate and the time for both open and closed boundary conditions is shown in Figure 4.4.

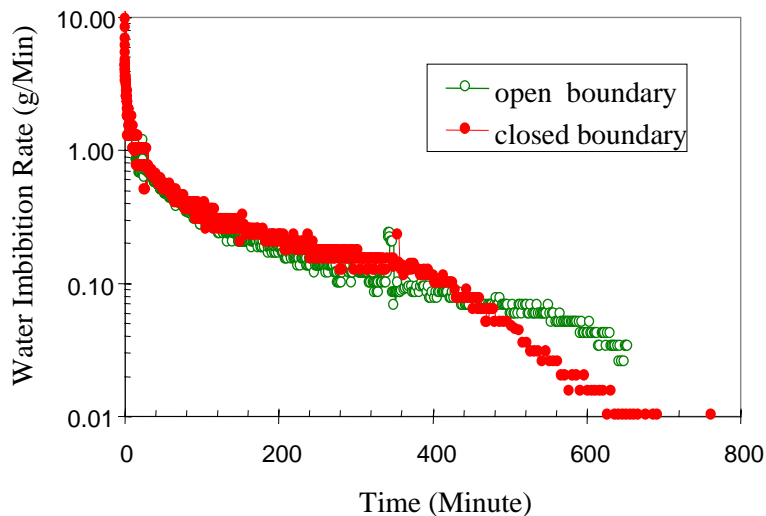


Figure 4.4: Water imbibition rate vs. time in sandstone.

The relationship between the water imbibition rate and the reciprocal of imbibition recovery for both open and closed boundary is plotted in Figure 4.5. It can be seen from Figure 4.5 that the water imbibition rate in the core with open conditions is greater than that with closed conditions. Comparing Figure 4.5 with Figure 4.4, the water imbibition rate is more sensitive to the reciprocal of imbibition recovery than to the imbibition time. This phenomenon also demonstrates that the relationship between the water imbibition rate and the reciprocal of imbibition recovery is appropriate for characterizing the imbibition behavior of water into rocks.

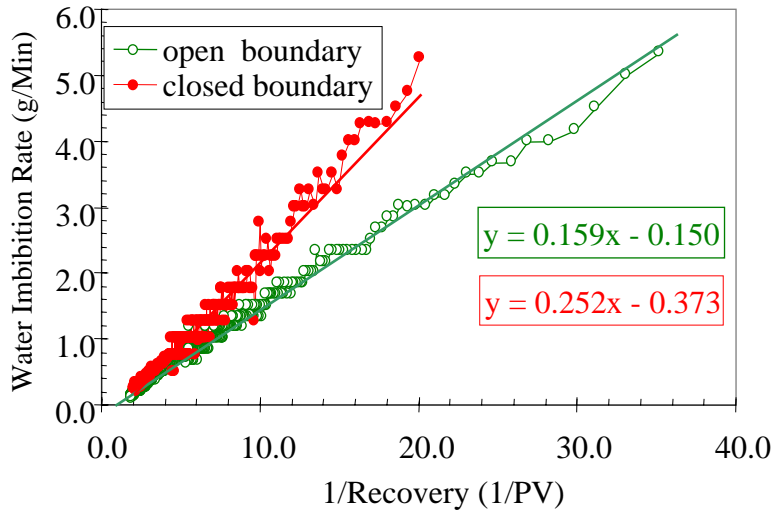


Figure 4.5: Water imbibition rate vs. reciprocal of production in sandstone.

After the water imbibition test in the core sample with the closed boundary condition, an initial water saturation was established to study the water imbibition behavior at different initial water saturations. The X-ray CT method was used to measure the distribution of water saturation in the core. Before the water saturation was measured, the porosity distribution in the core was measured by using the CT technique and is plotted in Figure 4.6. The porosity distribution in this core was homogeneous.

We first tried to establish an initial water saturation in the core by injecting only air. The direction of air flow was varied by injecting alternately from each end of the core. This technique for establishing initial water saturation worked well in a 10cm long sandstone core. However, it was not clear whether it was suitable for a 43.5cm long core sample. The distribution of water saturation in the core is shown in Figure 4.7, which shows that the water saturation was not homogeneous at any of the three water saturation values. The values of S_w shown in Figure 4.7 are the values of average water saturation in the core sample measured using the weight change of the core. Figure 4.7 shows that it is almost impossible to establish a homogeneous initial water distribution in a long core by only air injection. Therefore, we started to use a steady-state technique. Air and water were injected simultaneously into the core with a specific ratio of air to water flow rates.

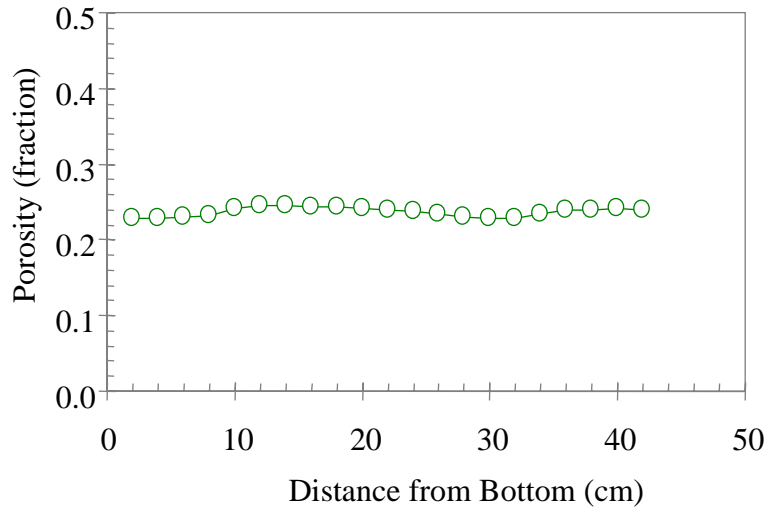


Figure 4.6: Porosity distribution in a sandstone sample.

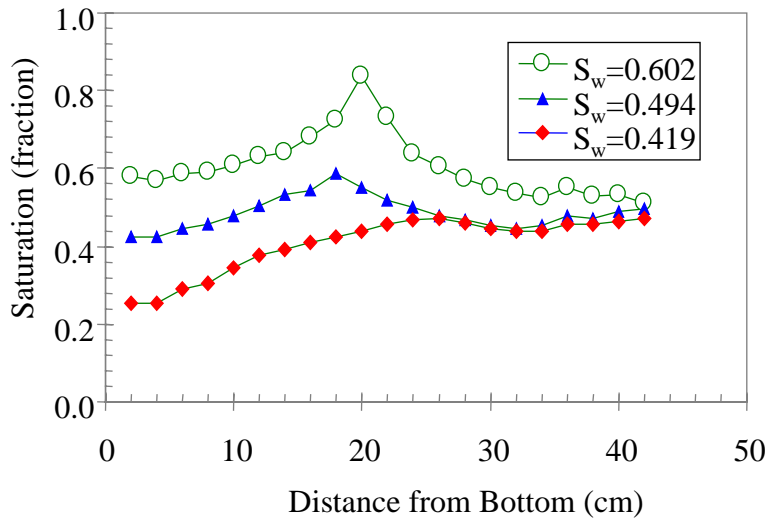


Figure 4.7: Distribution of water saturation in a sandstone sample by using single air injection.

Figure 4.8 shows the distribution of initial water saturation after steady state was reached in the core (open circle). Also shown in Figure 4.8 are the distributions of water saturation in the core after the water imbibition tests at different values of initial water saturation. Compared with the distributions of initial water saturation shown in Figure 4.7, it can be seen from Figure 4.8 that the steady state technique could establish more homogeneous distributions of water saturation than only air injection. Figure 4.8 also demonstrates that the distributions of water saturation in the core after water imbibition tests were not influenced significantly by the values of the initial water saturation.

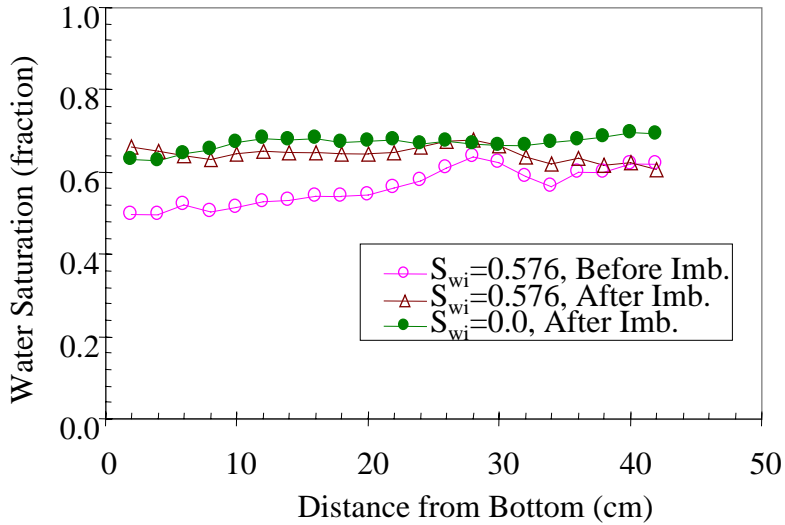


Figure 4.8: Distribution of water saturation in a sandstone sample by using a steady state technique.

After the initial water saturation in the core was established, water imbibition tests were conducted. The relationship of water gain vs. imbibition time is shown in Figure 4.9 for different values of initial water saturation.

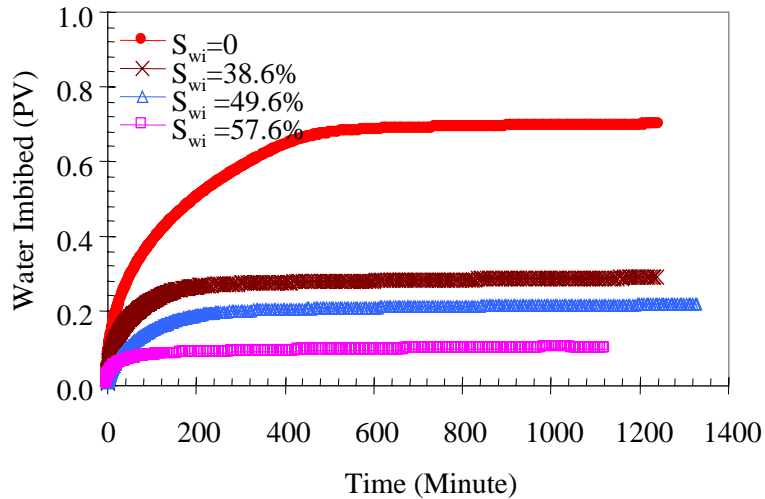


Figure 4.9: Water gain vs. time in sandstone at different initial water saturation.

It can be seen from Figure 4.9 that the amount of water imbibed into the core sample and the time that water gain reached the maximum value decreased with an increase of initial water saturation.

The water imbibition rate vs. the reciprocal of recovery is shown in Figure 4.10. The y-axis is the water imbibition rate and x-axis the reciprocal of recovery. This figure demonstrates that the relationship between the water imbibition rate and the reciprocal of

recovery in a sandstone sample with different values of initial water saturation (except one point) is linear as predicted by the mathematical model developed this quarter.

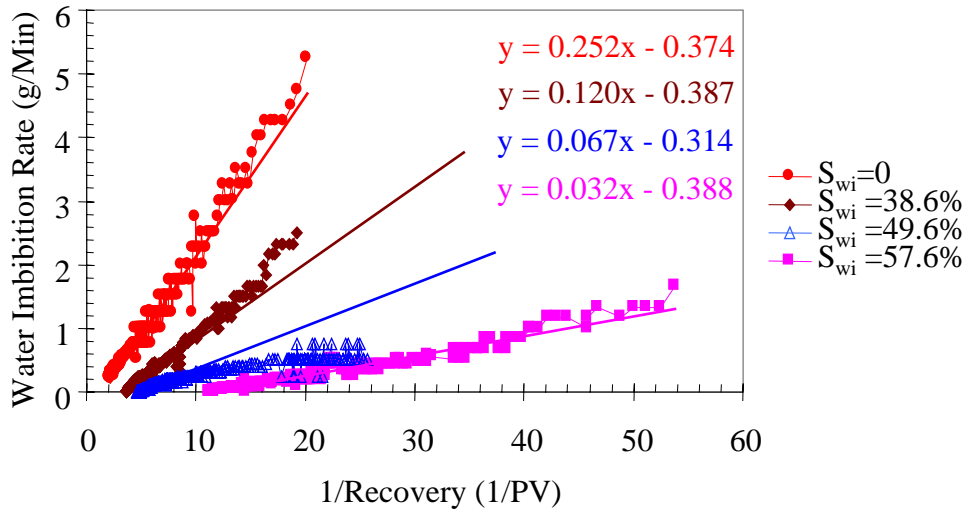


Figure 4.10: Water imbibition behavior at different values of initial water saturation in a sandstone sample.

At the initial water saturation of 49.6%, however, the relationship between the water imbibition rate vs. the reciprocal of recovery shown in Figure 4.10 is not linear. The reason for this phenomenon may be the heterogeneous distribution of initial water saturation in the core. The distributions of water saturation in the core before and after the water imbibition tests were measured using the X-ray CT technique and are plotted in Figure 4.11. For comparison, the distribution of water saturation in the core after water imbibition at zero initial water saturation (closed condition) is also shown in this figure. The distribution of initial water saturation with a value of 49.6% was not homogeneous in the region near the bottom where the water imbibition started. It took more than 40 hours to establish the initial water saturation by simultaneous injection of air and water from the top of the core. The heterogeneous distribution of initial water saturation shown in Figure 4.10 may be due to the capillary end effect in multiphase flow. The water saturation near the bottom region was about 63%, very close to the maximum water saturation (about 65%) that the imbibition could reach in this type of rock. This region with high water saturation would behave as a barrier for water imbibition, which would reduce the water imbibition rate at the beginning of the imbibition process.

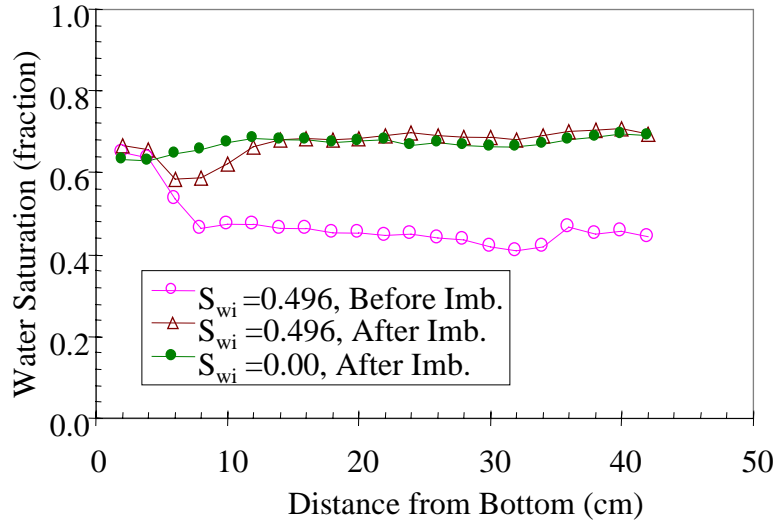


Figure 4.11: Distributions of water saturation in a sandstone core.

It can also be seen from Figure 4.11 that the distributions of water saturation after water imbibition at two different points of initial water saturation (0 and 0.496) were almost the same. In order to avoid the barrier (formed by a high water saturation region) for water imbibition, air and water were injected simultaneously from the bottom of the core sample to establish the other initial water saturation (0.376). This idea was based on the observation in Figure 4.11 that the distribution of water saturation from the injection point to the position about 3 cm away from the outlet was very homogeneous. The distributions of water saturation before and after water imbibition at the initial water saturation of 0.376 are shown in Figure 4.12.

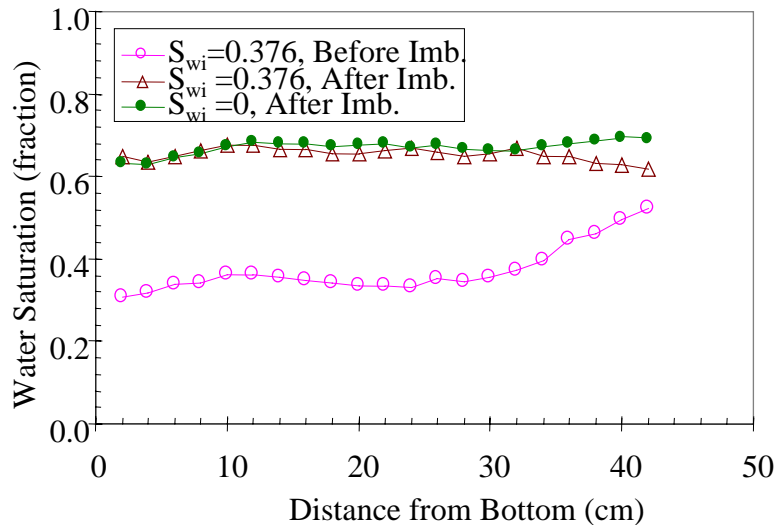


Figure 4.12: Distributions of water saturation in a sandstone core.

Figure 4.12 also shows that there was very little effect of initial water saturation on the distributions of water saturation after water imbibition in the core.

The relationship between the water imbibition rate and the reciprocal of recovery at the initial water saturation of 0.376 is almost linear except at the beginning of water imbibition (see Figure 4.10). The unusual high water imbibition rates at the beginning might have been brought about by the heterogeneous distribution of initial water saturation (see Figure 4.12).

The values of slope and intersection of the imbibition curves shown in Figure 4.10 were obtained by linear regression and the corresponding equations are also listed in this figure. Note that only the points in the later period of water imbibition at the initial water saturation of 0.496 were used to do the linear regression for calculating the values of the slope and the intersection. These values were used to calculate the corresponding capillary pressures using Equation 4.15. The calculated capillary pressure vs. initial water saturation is shown in Figure 4.13.

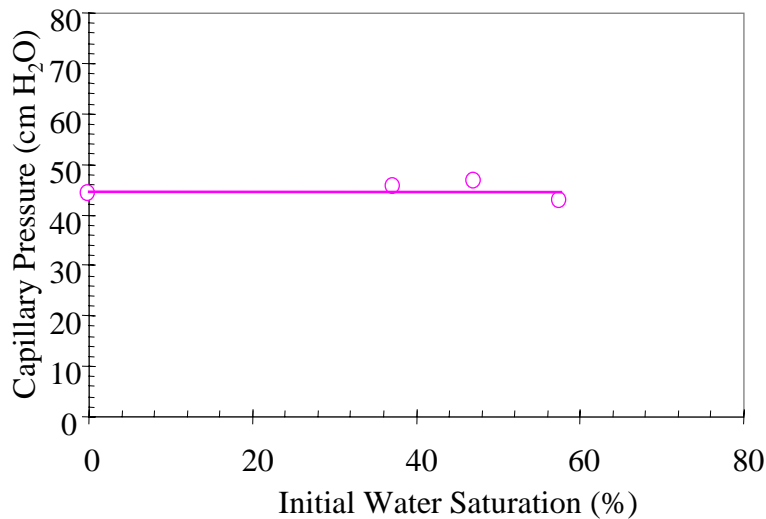


Figure 4.13: Capillary pressure vs. initial water saturation in a sandstone sample.

Although there are only four points in Figure 4.13, we can see that the capillary pressure was not influenced significantly by the initial water saturation over a wide range. This phenomenon may be explained as follows. It is the capillary pressure at the water saturation value behind the water imbibition front that controls the process of water imbibition instead of the capillary pressure at the water saturation value in front of the water imbibition front. The experimental results demonstrate that the water saturation behind the water imbibition front was almost unaffected by the initial water saturation. Otherwise, the relationship between the water imbibition rate and the reciprocal of recovery shown in Figure 4.10 would not be linear. Therefore, the capillary pressure calculated using Equation 4.15 does not change with the initial water saturation in the core.

The values of maximum water saturation or the imbibition recovery that could be reached by spontaneous water imbibition at different values of initial water saturation are shown in Figure 4.14.

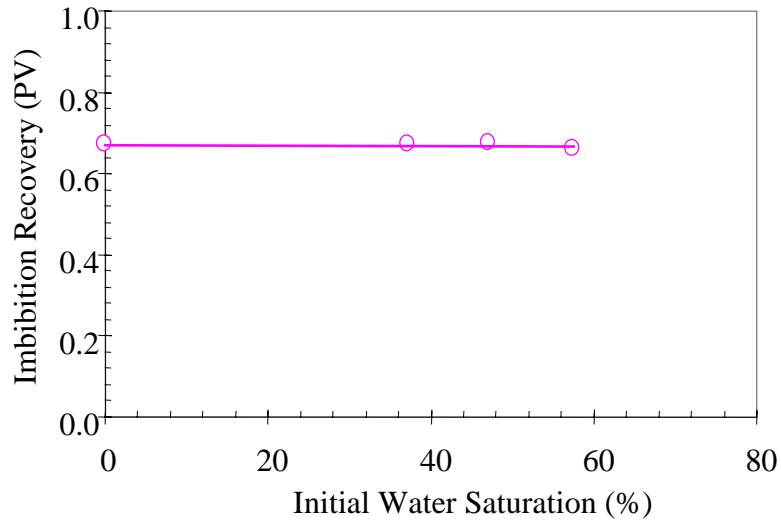


Figure 4.14: Imbibition recovery vs. initial water saturation in a sandstone sample.

It can be seen from Figure 4.14 that the maximum water saturation in the core or the imbibition recovery by spontaneous water imbibition did not vary much with initial water saturation. The maximum water saturation depends on rock permeability, pore structure, interfacial tension between two fluids, and wettability. Therefore, maximum water saturation by spontaneous water imbibition may be used as a parameter to estimate the ability of water injection into reservoirs.

Another interesting phenomenon observed in Figure 4.10 is that the value (b) of the intersection of the straight line changed very little with initial water saturation. Actually, the value of b should be constant because it depends only on the effective permeability (see Equation 4.13). The rock permeability is easy to measure; so the water relative permeability at residual gas saturation could also be calculated from the water imbibition test.

The physics that governs the water imbibition into porous media at different initial water saturation has actually been verified by the experimental results reported in the quarterly report for April-June 1999. To explain this, the water imbibition results in a glass-bead pack are cited here (see quarterly report for April-June 1999).

The water imbibition rate vs. the reciprocal of the production in a glass-bead pack is plotted in Figure 4.15.

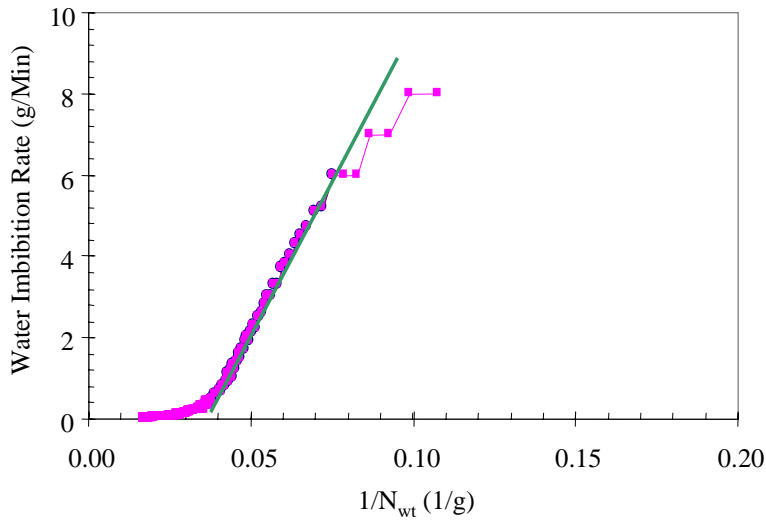


Fig. 4.15: Water imbibition rate vs. reciprocal of production in a glass-bead pack.

The relationship between the water imbibition rate and the reciprocal of production in a glass-bead pack (unconsolidated porous medium) is also linear over a certain period of the imbibition process (see Figure 4.15). The capillary pressure calculated using the linear relationship shown in Figure 4.15 is about 10 cm (water column). This value is the capillary pressure at the water saturation behind the water imbibition front. The air-water imbibition capillary pressure curve of the glass-bead pack measured using the X-ray CT method is plotted in Figure 4.16. Comparing Figure 4.15 with Figure 4.16, it is known from the experimental results that the linear part of the imbibition curve in Figure 4.15 corresponds to the maximum water saturation section in Figure 4.16. We can see from Figure 4.16 that the air-water capillary pressure at the water saturation behind the water imbibition front (actually the maximum water saturation) is about 10 cm (water column). Therefore, the capillary pressure calculated using Equation 4.15 with the values of the slope and the intersection of the imbibition curve is equal to that measured using an X-ray CT method for the same section from 0cm (bottom) to 10cm in the glass-bead pack.

The capillary pressure $P_c(S_{wmax})$ at the maximum water saturation shown in Figure 4.16 has some important features. First, all the water saturations at the capillary pressure less than $P_c(S_{wmax})$ have the same value. Secondly, the spontaneous water imbibition upward in a core with a length less than the water column height corresponding to $P_c(S_{wmax})$ may be piston-like and have a linear relationship between the imbibition rate and the reciprocal of recovery. This idea could be also applied to actual reservoirs. If water is injected into a geothermal reservoir with a height less than the water column height corresponding to $P_c(S_{wmax})$, there may be only one capillary pressure, $P_c(S_{wmax})$, that governs the process of water injection into the matrix.

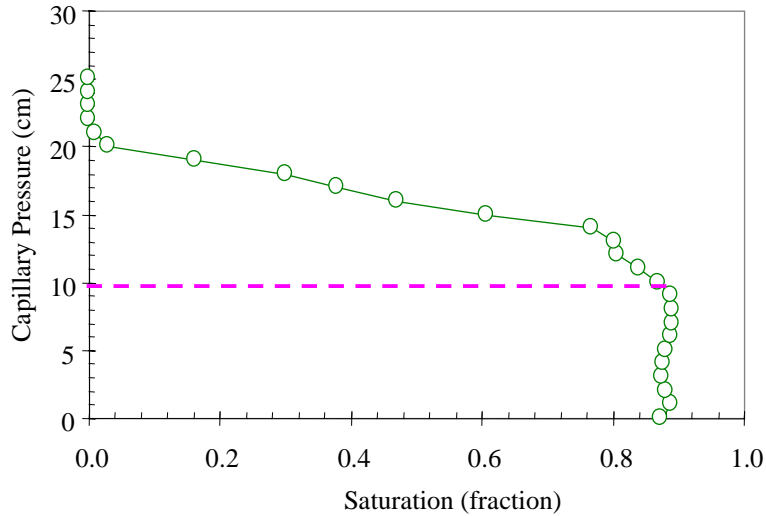


Figure 4.16: Air-water imbibition capillary pressure of a glass-bead pack measured using the X-ray CT technique.

4.5 DISCUSSION

Only one point of capillary pressure could be obtained from the spontaneous water imbibition test according to the study conducted this quarter. So we have to develop another method to measure steam-water capillary pressure curves. Since we observed that the maximum water imbibition height in the glass-bead pack was about 20 cm, we will develop an apparatus for measuring steam-water capillary pressure curve for a glass-bead pack using an X-ray CT technique. The permeability of the glass-bead pack is of the order of the permeability in a fracture. Therefore, the capillary pressure of a glass-bead pack may be considered to be similar to the capillary pressure in a fracture if we assume that the two systems have the same wettability. The next step is to develop a method for measuring steam-water capillary pressure curves in low permeability rocks.

The discovery that only one point of capillary pressure governs the process of water imbibition at different initial water saturation is important to the reservoir engineering of geothermal water injection. Spontaneous water imbibition is a major physical process during the water injection into a highly fractured geothermal reservoir. Knowing that spontaneous water imbibition depends on only one capillary pressure, we may just need to know one capillary pressure value for the matrix to do the corresponding reservoir engineering calculation, which could be done by water imbibition tests in steam-water systems.

There may be other significance to the discovery that only one point of capillary pressure and water relative permeability at residual gas saturation govern the water imbibition behavior at different initial water saturations. Since only one point of capillary pressure and water relative permeability govern the water imbibition behavior, it may not be reasonable to infer the whole capillary pressure and relative permeability curves from the water imbibition (even water injection) tests in air-saturated rocks by using the technique

of automatic history matching. This type of method has been often used in reservoir engineering. One common phenomenon in the application of automatic history matching to infer capillary pressure and relative permeability curves is multiple solutions. That only one point of capillary pressure and water relative permeability governs the water imbibition behavior may be one of the reasons for the multiple solution problem.

How much is the difference between air-water and steam-water capillary pressure? This is a question that we have to answer for this project. Since it is more difficult to measure steam-water capillary pressure curves, it may be a good idea to compare the difference of water imbibition behavior in air-water systems with that in steam-water systems. To do so, we can conduct water imbibition tests (using the same core) in air-water and steam-water systems, respectively. If there were significant differences of capillary pressure between air-water and steam-water systems, the water imbibition behavior subject to calibrated for surface tension would also be significantly different. We can also obtain the capillary pressure and the relative (effective) permeability of water phase at the residual steam saturation from the water imbibition test. On the other hand, the imbibition recovery, dimensionless water imbibition rate, the capillary pressure, and the relative permeability at the residual steam saturation that were calculated from water imbibition tests in steam-water systems may be directly used to estimate the behavior of water or condensate injection into geothermal reservoirs.

4.6 CONCLUSIONS

Based on the work performed this quarter, the following conclusions may be drawn:

1. The relationship between water imbibition rate and the reciprocal of recovery is linear at different values of initial water saturation from 0 to 0.576.
2. The air-water capillary pressure (calculated using our analytical method) at the water saturation behind the imbibition front is equal to that measured by the X-ray CT technique for the imbibition in a glass-bead pack.
3. The maximum water saturation by water imbibition or the imbibition recovery is almost unaffected by initial water saturation in the core.
4. The process of water imbibition into porous media at different values of initial water saturation may be governed by only one capillary pressure, that is, the capillary pressure at the water saturation behind the imbibition front.
5. We could obtain only one point of capillary pressure even though we ran water imbibition tests at different values of initial water saturation.
6. The capillary pressure and the relative permeability of water phase at residual gas saturation could be calculated separately from the spontaneous water imbibition tests, which has not been reported previously.

4.7 FUTURE WORK

We will develop an apparatus to measure steam-water capillary pressure curve in a glass-bead pack or a highly permeable artificial rock by using an X-ray CT technique. We are also planning to develop a method for measuring steam-water capillary pressure curve in low permeability geothermal reservoir rocks.

5. ACCURATE MEASUREMENT OF STEAM FLOW PROPERTIES

This research project is being conducted by Research Associate Kewen Li and Professor Roland Horne. The objective of this project is to study the effect of gas slippage on steam-water relative permeability measurements. In this summary, we report on the reproducibility of the experimental values of steam slip factors at different temperatures.

5.1 SUMMARY

Using a modified apparatus for measuring steam slip factors, we repeated the measurements of the steam slip factors on the same core used last quarter and also on another core to verify the experimental results. The effect of temperature on steam slip factor was also investigated. It was found that the intrinsic permeabilities of steam calculated from the data at different test temperatures were consistent with the absolute permeability measured using NaCl brine of one percent (wt).

5.2 INTRODUCTION

We last reported on the effect of temperature on both nitrogen and steam slip factors in the quarterly report for April-June 1999. It was found in the last quarter that the unusual values of gas phase or steam phase relative permeabilities were attributable to the gas slip (Klinkenberg) effect in steam-water two-phase flow. The intrinsic permeabilities of nitrogen computed from the data at all the test temperatures were consistent with the absolute permeability measured using 1% (wt) brine. Those of steam, however, were much lower than the absolute permeability. To find the reason for this phenomenon, we modified the apparatus by installing a condenser at the outlet of the coreholder outside the oven to monitor the production rate of steam. An advanced water pump (Dynamax, Model SD-200) was used in this study to replace the old water pump (ConstaMetric, Model III) used last quarter.

5.3 EXPERIMENTS

Distilled water was used to generate steam needed for the measurement of steam permeability; the specific gravity and viscosity were 1.0 and 1.0 cp at 20°C. The steam properties at high temperatures were calculated with the values of pressure and temperature using steam tables. One of the cores used in this study was the same as that described in the last quarterly report. The permeability and porosity of the rock were 1280 md and 23.4%, respectively; the length and diameter were 43.2 cm and 5.08 cm. Another core was a Berea fired at a high temperature; its permeability and porosity were 1460 md and 24.7%; the length and diameter were 43.2 cm and 5.04 cm, respectively. This core and its coreholder were the same as used by Mahiya (1999).

Figure 5.1 shows a schematic of the apparatus modified for measuring the steam slip factor at high temperatures. The steam generator was a heater with a power of 500 W. The power required to generate steam was calculated roughly according to the flow rate of water injection and the temperatures of water and steam and then applied to the steam generator. To make sure that the injected cold water was generated to steam, a coil of stainless steel tubing with a length of about 2 m was installed in the oven between the

steam generator and the inlet of the core. The balance (Model BP6100) shown in Figure 5.1 was manufactured by Sartorius Corporations and used to monitor the water saturation in the core sample; this balance has an accuracy of 0.1g and a range from 0 to 6100 g.

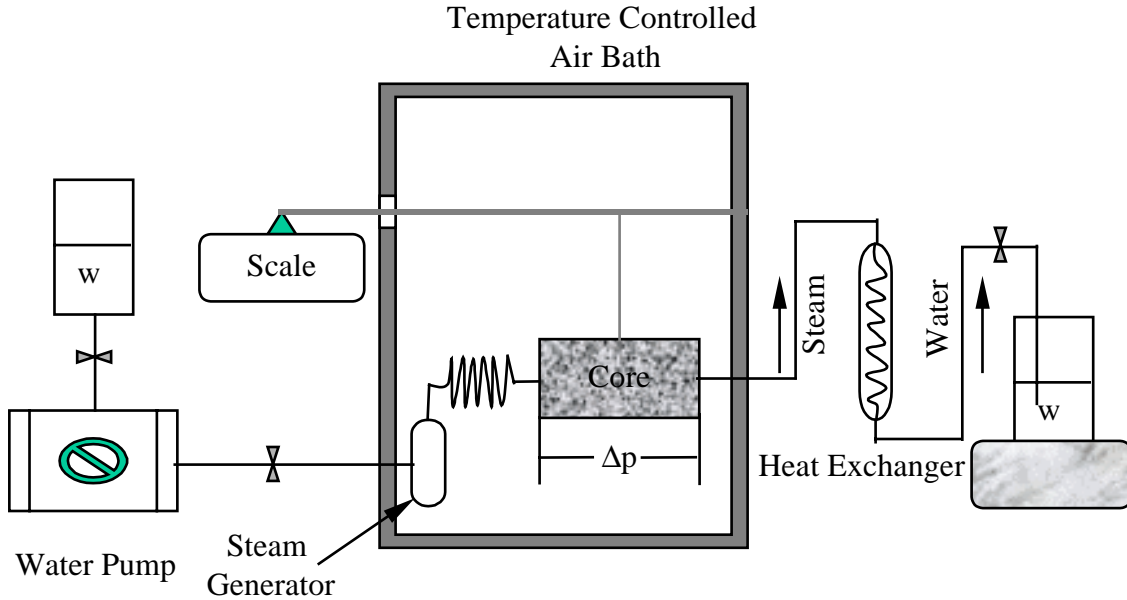


Figure 5.1: Schematic of apparatus for measuring steam slip factor.

A condenser was installed outside the oven at the outlet of the coreholder to monitor the production rate of steam. The pump (Dynamax, Model SD-200) used to inject distilled water was manufactured by RAININ Instrument Co., Inc; the minimum pumping flow rate is 0.05 ml/min with an accuracy of 0.01 ml/min. This pump is an automated constant-rate pump. The flow rates of the water pump were calibrated before the experiment using a stop-watch and a Mettler balance (Model PE 1600). The accuracy of the balance is 0.01g and a range from 0 to 1600 g. The calibration curve for this pump at room temperature is shown in Figure 5.2. The measured flow rates were consistent with those specified on the pump.

The flow rate of steam was calculated using the water injection rate and the density of steam at the temperature and pressure measured during the experiment.

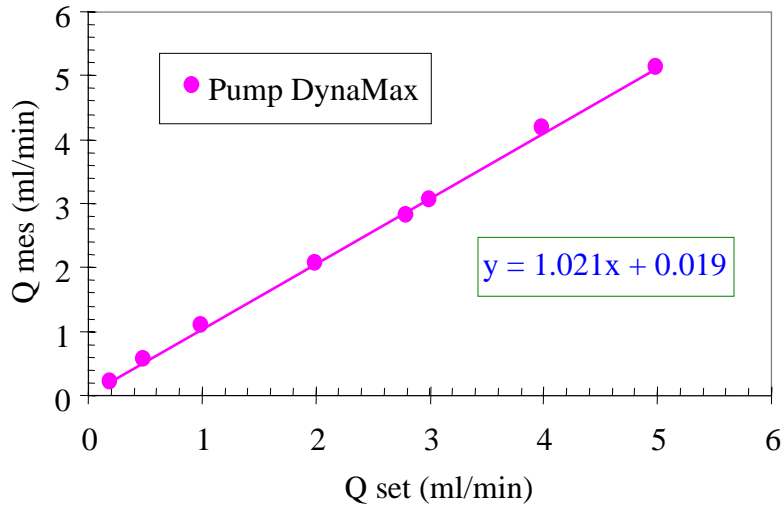


Figure 5.2: Calibration of flow rate for DynaMax pump.

The pressure across the core sample was measured using a differential pressure transducer manufactured by Celesco Company; this transducer (Model DP30) has a linearity of 0.5% and a repeatability of 0.5% full scale. The diaphragm used in this study has a range from 0 to 10 psi. This differential pressure transducer was checked using a pressure gauge with an accuracy of 0.1 psi. Figure 5.3 plots the measured data.

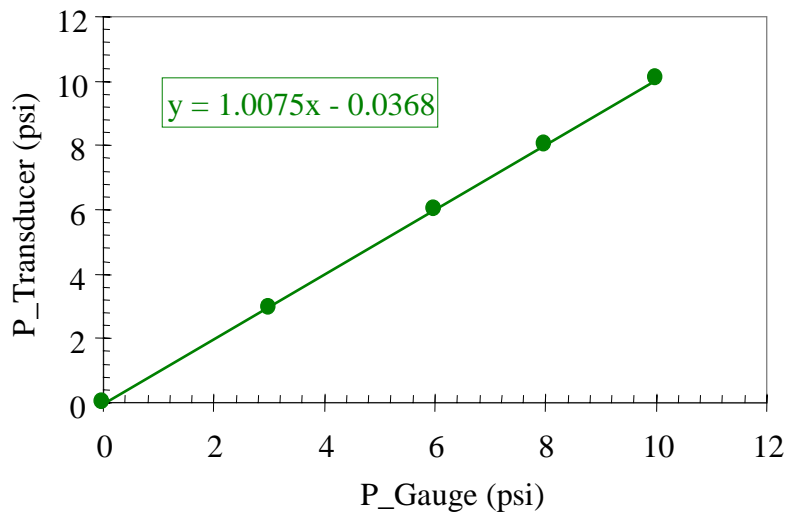


Figure 5.3: Calibration of differential pressure transducer.

The x-axis in Figure 5.3 is the pressure measured by the pressure gauge and y-axis the pressure measured by the transducer. It can be seen from Figure 5.3 that the measurements of pressure are in good agreement.

The coreholder and the method to assemble the core sample used in this study were similar to those of Satik and Horne (1998).

In order to repeat the experimental results, we measured the steam slip factor using another core with a permeability of 1460 md. The core and the coreholder were the same as used by Mahiya (1999). The temperature in this system was controlled automatically by using LabView 4.1 (National Instrument Co.) through flexible guard heaters that were wrapped around the coreholder. The schematic of this system for measuring the steam slip factor at high temperatures is shown in Figure 5.4.

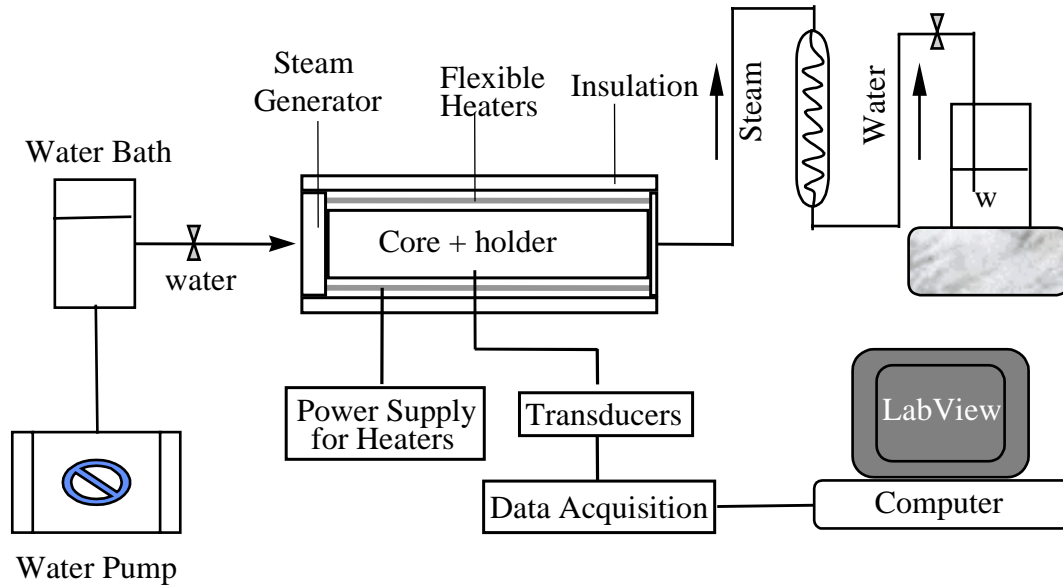


Figure 5.4: Schematic of apparatus for measuring steam slip factor using flexible heaters.

Using the apparatus shown in Figure 5.1, we found that the differential pressure across the core fluctuated very much and took long time to stabilize. To find a solution to this problem, we installed a constant-temperature water bath (Model 1136, manufactured by VWR Scientific Co.) before the built-in steam generator to increase the temperature of the water to about 98°C. Thus, the difference of temperature between the water before entering the heater and the steam after injecting into the core was reduced. This reduction of temperature difference was helpful in stabilizing the differential pressure across the core. The experimental results showed that the time needed to stabilize the differential pressure across the core was significantly reduced.

Pressure and temperature were measured through ports at eight positions along the core spaced about 5 cm apart. To calculate steam slip factor, we used the data of the inlet and outlet pressures. The pressure transducers were calibrated before and after the experiments using a pressure gauge with an accuracy of 0.05 psi. The calibration curves of the inlet and outlet pressure transducers are shown in Figure 5.5. The x-axis in Figure 5.5 is the pressure measured by the pressure gauge and y-axis the pressure measured by the transducer.

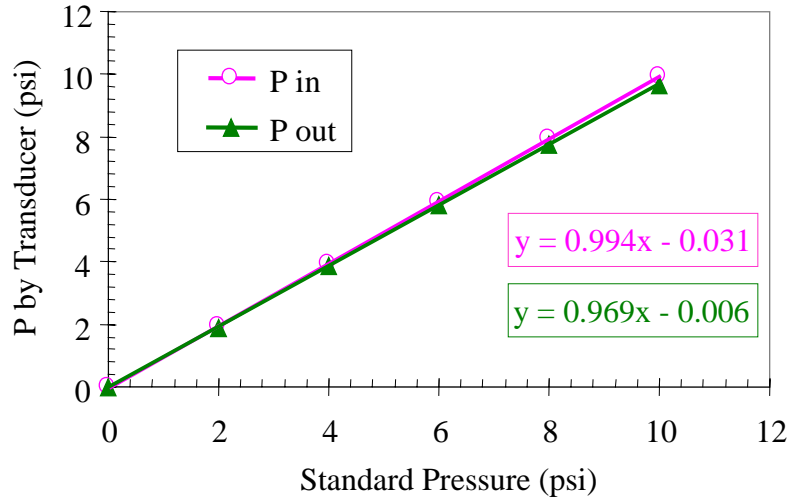


Figure 5.5: Calibration of pressure transducers at inlet and outlet.

It can be seen from Figure 5.5 that the values of pressure measured by the pressure transducers at the inlet and outlet were consistent with those measured by the standard pressure gauge with a high accuracy.

The core was first dried by evacuation. The weight of the coreholder was monitored using the Sartorius balance with an accuracy of 0.1 g. The core was assumed to be dry when the weight did not change in eight hours of evacuation at a vacuum of about 30 millitorr. Once dried, the core was evacuated again to remove the air inside the rock. The injection of steam was then started at a temperature greater than 100°C. The steam permeabilities were measured at different mean pressures by varying the water injection rate after the differential pressure across the core was stabilized. The saturation pressure at the experimental temperature was calculated and the maximum steam injection rate was then computed roughly using Darcy's law. The steam injection rate needed to be less than the calculated maximum flow rate at that temperature. Following that, the core was heated and the steam permeabilities were measured again at a higher temperature. The slip factor of steam was calculated using the measured steam permeabilities at different mean pressures.

5.4 RESULTS

Steam slip factors of the two cores were measured at different temperatures using the modified apparatus. It was found that there was a significant effect of temperature on steam slip factor.

The steam slip factors in the rock with permeability of 1280 md using the apparatus shown in Figure 5.1 are demonstrated in Figure 5.6. The slip factor of steam was measured at three different temperatures (120.1°C, 150.8°C, and 170.2°C). It is seen from Figure 5.6 that the steam permeabilities at specific pressures increase with temperature. The intrinsic permeabilities of steam at the two different temperatures are almost equal to each other and close to the absolute permeability measured by brine injection.

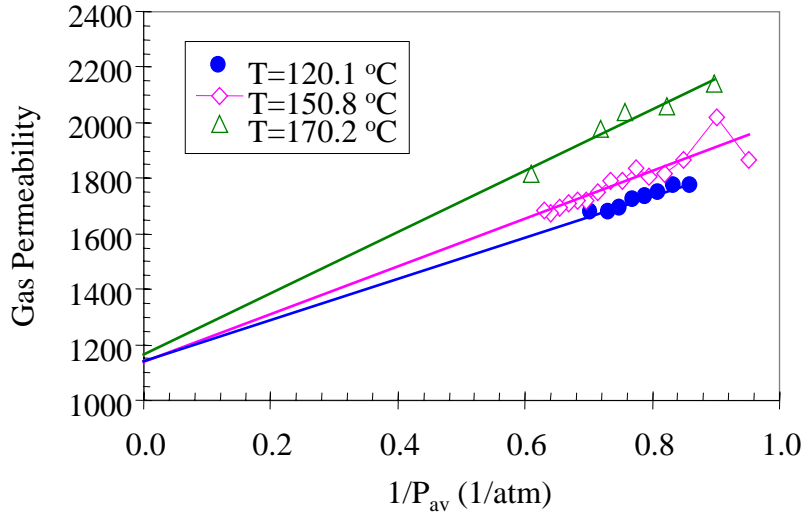


Figure 5.6: Effect of temperature on steam permeabilities and slip factor.

The values of steam slip factor at different temperatures are listed in Table 5.1. It can be seen that the value of steam slip factor at high temperature is greater than that at low temperature. During these experiments, the production rates of steam were measured and were confirmed to be equal to the injection rates. Comparing the values of steam slip factor to those reported in the last quarterly report, the values of steam slip factor measured this quarter using the modified apparatus were smaller.

Table 5.1: Steam slip factors at different temperatures.

Temperature (°C)	120.1	150.8	170.2
Steam slip factor (atm)	0.642	0.749	0.948

These experiments yielded values of the intrinsic permeabilities of steam (the intercept values in Figure 5.6) that were very close to the absolute permeability of the core. Therefore, the values of steam slip factor listed in Table 5.1 should be close to the actual values for this core.

The relationship between steam slip factor and temperature for the second core (with a permeability of 1280 md) is shown in Figure 5.7. Although there are only three points, the trend is clear. That is, the slip factor increases with the increase of test temperature. This relationship as shown in Figure 5.7 may be used to estimate the steam slip factors at different temperatures.

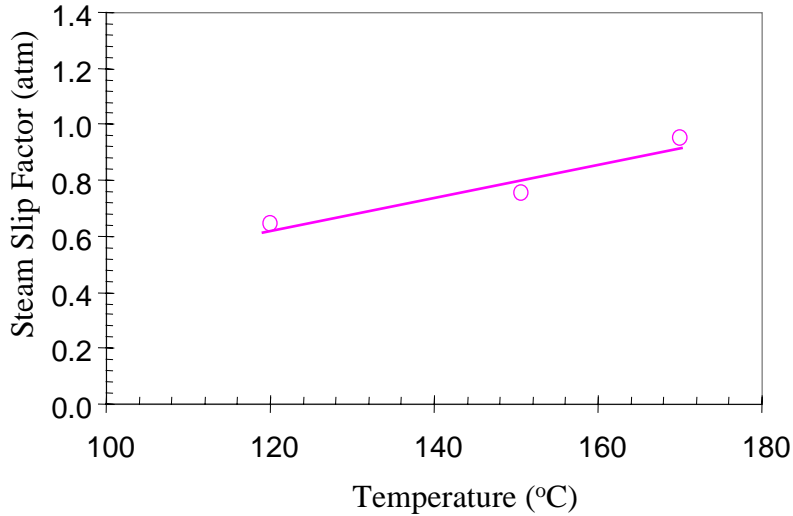


Figure 5.7: Relationship between steam slip factor and temperature.

Another measurement for the steam slip factor of the second core was made using the apparatus shown in Figure 5.4. The injection and production rates of steam through the core were monitored during the experiment. Figure 5.8 shows the comparison of the steam flow rates at the inlet with those at the outlet of the core.

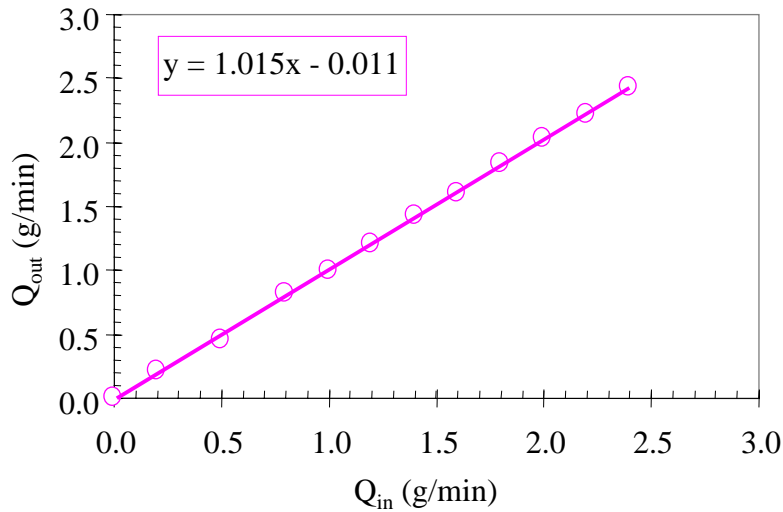


Figure 5.8: The comparison of the steam flow rates at the inlet with those at the outlet of the core.

It can be seen from Figure 5.8 that the production rates of steam are equal to the injection rates.

The slip factor of nitrogen on this core was measured at a room temperature and is plotted in Figure 5.9. The method for measuring nitrogen slip factor was the same as that reported in the last quarterly report. The flow rates of nitrogen were controlled and measured using a mass flow rate controller manufactured by Matheson Company.

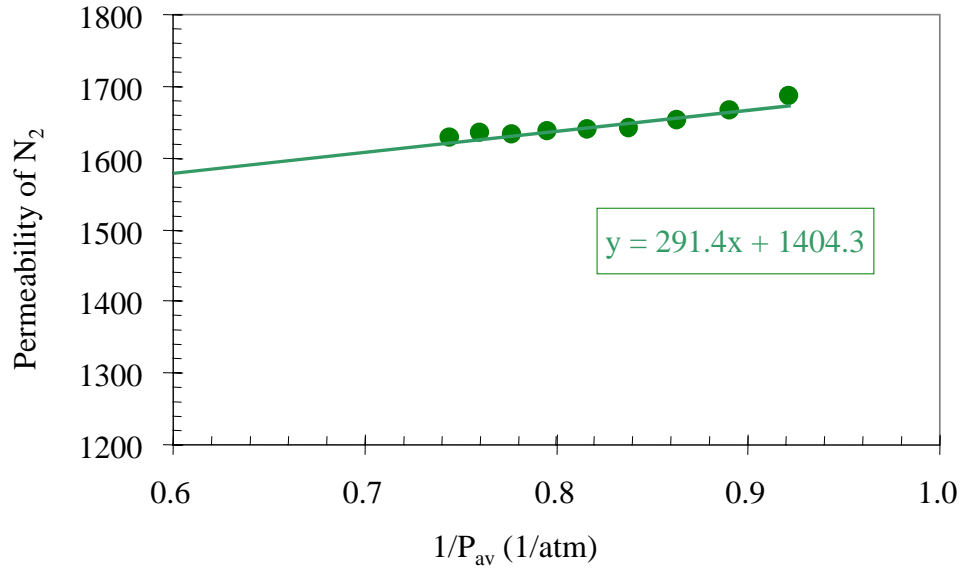


Figure 5.9: The slip factor of nitrogen in the core with permeability of 1460 md at room temperature.

The intrinsic permeability measured using nitrogen (the intercept is to the left of the range shown in Figure 5.9) is very close to the absolute permeability of this core (1460 md). The slip factor of nitrogen calculated from the experimental data shown in Figure 5.9 is about 0.208 atm. This value is less than that of the first core with permeability of 1280 md, which is reasonable since the slip factor usually decreases with the increase of absolute permeability.

Following the measurement of the nitrogen slip factor, the core was evacuated again to remove the nitrogen inside the core. The steam injection was then started after the system temperature was raised to 120.1°C. The steam slip factor measured at this temperature is shown in Figure 5.10. The intrinsic permeability measured using steam injection (see Figure 5.10) is close to the absolute permeability of this core. The steam slip factor calculated from the data shown in Figure 5.10 is 0.251 atm. This value is less than the steam slip factor of the core with permeability of 1280 md at the same temperature (see Figure 5.6), which is not surprising because the permeability of this core is greater than that of the core used in Figure 5.6.

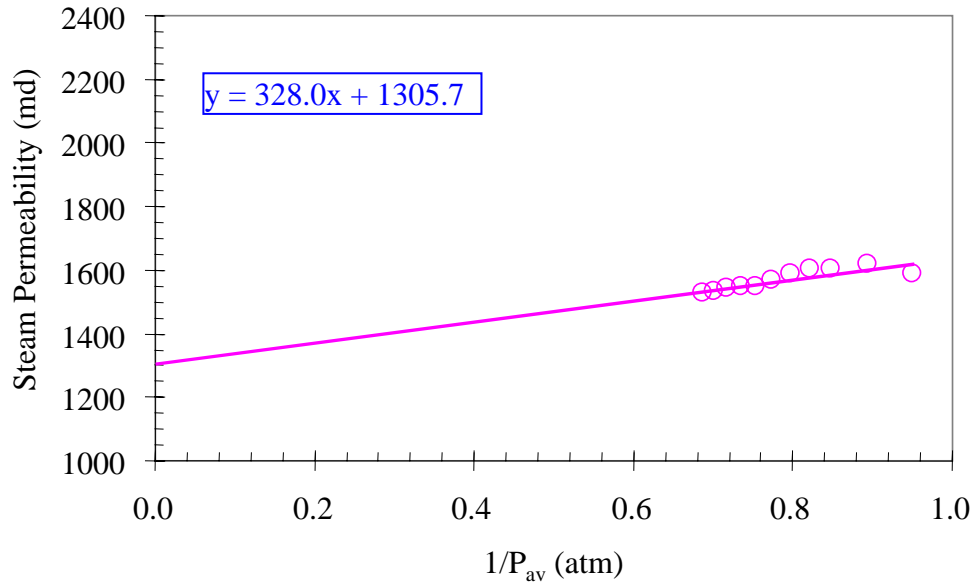


Figure 5.10: The slip factor of steam in the core with permeability of 1460 md at a temperature of 120°C.

5.5 CONCLUSIONS

Based on the present work, the following conclusions may be drawn:

1. More reliable values of steam slip factor on two different cores were measured at different temperatures using modified apparatus.
2. Steam slip factor decreases with an increase of absolute permeability. Steam slippage is significant even in a highly permeable rock and will need to take into account when calculating steam relative permeabilities from experimental data.
3. The effect of temperature on the steam slip factor is also significant. The steam slip factor increases with an increase of temperature.

5.6 FUTURE WORK

We will start to measure relative permeabilities of steam and water at different mean test pressures but at the same flow rates. Subsequently the slip factors of steam at different water saturations will be calculated.

6. REFERENCES

Ambusso, W., Satik, C., and Horne, R. (1996), "A Study of Relative Permeability for Steam-Water Flow in Porous Media", Proceedings of 21st Workshop on Geothermal Reservoir Engineering, Stanford University, Stanford, California.

Grant, M. (1979) "Water Content of the Kawah Kamojang Geothermal Reservoir", Geothermics, Volume 8, pages 21-30.

Guerrero, M., Satik, C., Finsterle, S., and Horne, R. (1998), "Inferring Relative Permeability From Dynamic Boiling Experiments", Proceedings of 23rd Workshop on Geothermal Reservoir Engineering, Stanford University, Stanford, California.

Horne, R. (1991), Notes on Geothermal Reservoir Engineering, Stanford University, Stanford, California.

Li, K., and Horne, R.N.: Accurate Measurement of Steam Flow Properties, *GRC Trans.* 23 (1999).

Mahiya, G. and Horne, R. (1998), "Measurements of Steam-Water Relative Permeability", Stanford Geothermal Program Quarterly Report April-June 1998, Stanford University, Stanford, California.

Mahiya, G.F.: *Experimental Measurement of Steam-Water Relative Permeability*, MS report, Stanford University, Stanford, CA (1999).

Satik, C. (1998), "A Measurement of Steam-Water Relative Permeability," Proceedings of 23rd Workshop on Geothermal Reservoir Engineering, Stanford University, Stanford, California.

Schembre, J.M., Akin, S., Castanier, L.M., and Kovsky, A.R.: "Spontaneous Water Imbibition into Diatomite," paper SPE 46221, presented at the 1998 Western Region Meeting, Bakersfield, California, May 10-13.

Satik, C. (1997), "Experiments of Boiling in Porous Media", Proceedings of 22nd Workshop on Geothermal Reservoir Engineering, Stanford University, Stanford, California.

Satik, C. (1998), "A Measurement of Steam-Water Relative Permeability", Proceedings of 23rd Workshop on Geothermal Reservoir Engineering, Stanford University, Stanford, California.